



HAL
open science

Bathymetric Controls on Rotational Surfzone Currents

R. Jak Mccarroll, Robert W. Brander, Tim Scott, Bruno Castelle

► **To cite this version:**

R. Jak Mccarroll, Robert W. Brander, Tim Scott, Bruno Castelle. Bathymetric Controls on Rotational Surfzone Currents. *Journal of Geophysical Research: Earth Surface*, 2018, 123 (6), pp.1295-1316. 10.1029/2017jf004491 . hal-04569123

HAL Id: hal-04569123

<https://hal.science/hal-04569123v1>

Submitted on 16 May 2024

HAL is a multi-disciplinary open access archive for the deposit and dissemination of scientific research documents, whether they are published or not. The documents may come from teaching and research institutions in France or abroad, or from public or private research centers.




L'archive ouverte pluridisciplinaire **HAL**, est destinée au dépôt et à la diffusion de documents scientifiques de niveau recherche, publiés ou non, émanant des établissements d'enseignement et de recherche français ou étrangers, des laboratoires publics ou privés.

Copyright

RESEARCH ARTICLE

10.1029/2017JF004491

Bathymetric Controls on Rotational Surfzone Currents

R. Jak McCarroll¹ , Robert W. Brander², Tim Scott¹ , and Bruno Castelle^{3,4} 

Key Points:

- Lagrangian data across seven flow regimes used to determine how bathymetric variations affect flow behavior within the surfzone
- Bathymetric variability correlated with mean velocity, and inversely with directional variability, channel angle controls eddy direction
- Flow continuum found from alongshore uniform morphology transient eddies, to rip channelled mean currents, modulated by channel geometry

Supporting Information:

- Supporting Information S1
- Data Set S1
- Data Set S2
- Data Set S3
- Data Set S4
- Data Set S5
- Data Set S6
- Data Set S7
- Data Set S8

Correspondence to:

 R. J. McCarroll,
 jak.mccarroll@plymouth.ac.uk

Citation:

 McCarroll, R. J., Brander, R. W., Scott, T., & Castelle, B. (2018). Bathymetric controls on rotational surfzone currents. *Journal of Geophysical Research: Earth Surface*, 123, 1295–1316. <https://doi.org/10.1029/2017JF004491>

Received 10 SEP 2017

Accepted 10 APR 2018

Accepted article online 27 APR 2018

Published online 15 JUN 2018

¹Coastal Processes Research Group, School of Biological and Marine Sciences, University of Plymouth, Plymouth, UK,²School of Biological, Earth and Environmental Sciences, UNSW Australia, Sydney, New South Wales, Australia, ³University Bordeaux, UMR EPOC, Pessac, France, ⁴CNRS, UMR EPOC, Pessac, France

Abstract A multibeach Lagrangian data set was used to determine bathymetric controls on flow variability within the surfzone. Seven microtidal flow regimes were examined, six containing rip channels, under moderate shore normal waves. Three selected zones exemplified varying bathymetric control: (i) a alongshore uniform zone; (ii) a shallow rip channel at an oblique angle to shore normal; and (iii) a deep, shore-normal rip channel. Bathymetric variables included alongshore nonuniformity (φ) and channel angle relative to shore normal (α). Low-frequency flow (0.01 Hz) was described by velocity (U), velocity standard deviation (σ_U), angular deviation (σ_θ), and bias in direction of eddy rotation (ζ_{bias}). Observations of the exemplar zones indicated the following: (i) near-zero mean flow with transient eddies within the alongshore uniform zone; (ii) low mean flow with high ζ_{bias} within the oblique channel; and (iii) strong mean flow with low ζ_{bias} in the deep channel. Bathymetry and flow variables were spatially averaged and linearly correlated, scaling for wave forcing. Normalized flow variables were found to be interdependent and were correlated with bathymetric variability, with $[U \propto \varphi]$, $[(U/\sigma_U) \propto \varphi]$, and $[\sigma_\theta \propto -\varphi]$, all with ($R^2 \geq 0.8$). A correlation was determined between α and ζ_{bias} ($R^2 \geq 0.7$, increasing as zone width is decreased), with peak ζ_{bias} within oblique channels. Based on these results, a conceptual model is introduced to predict flow behavior for known bathymetry. Surfzone currents were found to span a dynamic continuum from transient eddies on alongshore uniform bathymetry, to channelized rip currents, forced by bathymetric three-dimensionality and mediated by channel geometry.

1. Introduction

Horizontal rotational currents in the surfzone result from alongshore variations in wave forcing (Castelle, Scott, et al., 2016; MacMahan et al., 2006). Two types of rotational surfzone currents of interest in this study are: (i) channelized rip currents and (ii) transient surfzone eddies. Channelized rip currents are forced by three-dimensional bathymetry that systematically modifies the wavefield (Dalrymple et al., 2011; Sonu, 1972). Transient surfzone eddies, absent of any bathymetric control, are generated by random variations in a directionally spread wavefield (Peregrine, 1998). Both forms of current exhibit nonzero vertical vorticity (MacMahan, Reniers, et al., 2010; Spydell & Feddersen, 2009), that is, they are rotational, and may be distinguished by displaying either a mean nonzero velocity (channelized rip currents) or, alternatively, transient with near-zero mean velocity when averaged at a given location (surfzone eddies). On natural beaches, channelized rip cell circulation is always a combination of mean and variable flows (MacMahan et al., 2004b). Other forms of surfzone currents, not of direct interest here, include alongshore currents generated by oblique waves, bed return flow, boundary currents controlled by headlands or structures (Castelle, Scott, et al., 2016), and nonrotational infragravity motions (MacMahan et al., 2004a).

The forcing mechanisms for mean rip flows over bar-rip channel systems are well understood and are traditionally explained using the concept of momentum flux due to waves, described as radiation stress (Bowen, 1969; Longuet-Higgins & Stewart, 1964). In a typical scenario with shallow shore-connected bars interspersed with deeper rip channels (e.g., MacMahan et al., 2005), increased dissipation due to wave breaking over the bars produces greater cross-shore radiation stress gradients forcing onshore flow and increased setup at the shoreline. An alongshore pressure gradient near the shoreline, from regions of higher to lower dissipation, drives a current toward the rip channel and offshore. Other efforts have focused on what occurs as a rip flows offshore, encountering opposing onshore forcing and exchanging energy with waves (e.g., Yu & Slinn, 2003). If waves are regularly breaking over a rip head bar, then roller forcing will likely recirculate the current within the surfzone in an enclosed eddy (Pitman et al., 2016; Reniers et al., 2007). Conversely, if waves are small, the surfzone is narrow and breaking is absent at the head of the rip channel; the mean flow is more likely to exit offshore beyond the surfzone (Scott et al., 2014).

An alternative approach to derive the forcing balance for mean rip cell flow is to directly define vorticity generation over a phase-averaged wave dissipation field (Bonneton et al., 2010). Peregrine (1998) determined that for a breaking wave where only part of the crest is broken, vorticity is generated from the breaking section around through the unbroken crest, to the back of the wave, later confirmed in the field by Clark et al. (2012). For a phase-averaged bar-rip system, this approach of direct vorticity generation can reproduce observed rotational flow by estimating vorticity diffusion (Bruneau et al., 2011), without the need to determine momentum flux and water level gradients.

The dynamics of channelized rip cells have been extensively studied, and the forcing controls on mean flow are reasonably well understood (Castelle, Scott, et al., 2016). Channelized rip mean velocities scale with increased wave energy (Brander & Short, 2000; Bruneau et al., 2009; MacMahan et al., 2006, 2005) and increased depth of the channel relative to the bar, with this depth ratio increasing at lower tidal levels (Austin et al., 2010; Scott et al., 2014; Sonu, 1972). These studies have typically examined flow for single points in a rip channel or adjacent bar; however, a generalized relationship between bathymetric three-dimensionality and mean flow across the surfzone is yet to be established. Rip channel width has been inversely correlated with flow velocity observations (MacMahan et al., 2006), and Castelle et al. (2014) numerically modeled the influence of rip spacing and rip head bar morphology on surfzone retention. Decreases in channel cross-sectional area may be related to increased rip flow, through morphological constriction (Austin et al., 2010; Brander, 1999). However, an objective method to examine the influence of other aspects of channel geometry on flow (e.g., channel obliquity) has not been determined.

While mean rip flows are well studied, variable flows forced by purely hydrodynamic controls have received less attention (Castelle, Scott, et al., 2016). Several recent efforts have focused on examining variable flows on alongshore uniform beaches (e.g., Feddersen, 2014; Spydell et al., 2007) where mean cross-shore flows, for a given spatial location, are absent at hourly time scales and rotational flows occur in the form of transient surfzone eddies that occasionally exit the surfzone as transient rip currents (Hally-Rosendahl et al., 2015; Johnson & Pattiaratchi, 2004, 2006). Transient surfzone eddies are generated by the vorticity forcing mechanism of short crested waves proposed by Peregrine (1998), primarily at the frequency of incident waves of stochastically varying height and direction (Feddersen, 2014). While the injection scale is short, the bulk of transient eddy energy is found at much longer length scales (>100 m; Feddersen, 2014) in the very low frequency range ($O[10 \text{ min}]$) (MacMahan, Reniers, et al., 2010), likely due to small eddies cascading into larger ones (Spydell & Feddersen, 2009). Low-frequency velocity standard deviation is a measure of "transient eddy velocity" (Spydell et al., 2014), which has been found to increase with wave height (MacMahan, Reniers, et al., 2010), while the average rate at which material leaves the surfzone scales with wave directional spread (Suanda & Feddersen, 2015), with mixing magnified by stratification (Kumar & Feddersen, 2017).

In comparison to mean flow controls in channelized rips and variable flow on alongshore uniform beaches, the interaction of variable and mean flows on 3-D morphology is poorly understood. Early studies noted the presence of fluctuations in rip velocity (e.g., Brander & Short, 2001; Sonu, 1972), and channelized rip flows are known to vary at infragravity and very low frequency time scales (MacMahan et al., 2006). Recent efforts have investigated variable rip behavior and the likelihood of a rip current to exit the surfzone (Castelle et al., 2014; MacMahan, Brown, et al., 2010; Pitman et al., 2016; Reniers et al., 2009; Scott et al., 2014), which has attracted interest due to implications for rip currents as a hazard. However, from a physical perspective, this is a specific aspect of the more generalized question as to how the forcing controls of wave energy interacting with 3-D morphology govern mean and variable flow behavior.

Field observations directly examining the interaction of transient surfzone eddies with mean channelized flows are few in number; notably, MacMahan et al. (2004b) determined that for a bar-rip system, with regularly spaced rip channels and transverse bars, very low frequency velocity variability (i.e., transient eddy velocity) peaks in the middle surfzone and is near constant alongshore. MacMahan et al. (2004b) also proposed a conceptual model where rip cells oscillate, mainly in the cross shore, due to the presence of transient eddies. However, other observations of rip currents radically changing trajectory, for example, by changing the direction of rotation (Castelle et al., 2010; Houser et al., 2013; Kennedy & Thomas, 2004), suggest that the model of rip cell oscillation is an incomplete description of the influence of

transient eddies on mean flows. A positive correlation has been determined between wave height and transient eddy velocity on a deeply rip channel beach (MacMahan et al., 2004b) and also between wave directional spread and transient eddy velocity for a shallow rip channel (MacMahan et al., 2008). However, no attempt has been made to compare transient eddy velocity for channels of varying depths and geometries in the field.

A laboratory study over a moveable sandy beach that underwent a “down-state” transition from a higher-energy more dissipative beach state to a lower-energy more reflective state (Castelle et al., 2010) attempted to address the impact of bathymetric three-dimensionality on flow behavior, observing that rip currents in deep channels are highly pulsating and weakly directionally variable, with flows becoming weakly pulsating and strongly directionally variable as alongshore bathymetric nonuniformity decreased. Brander (1999) observed a full down-state transition in the field, identifying a negative correlation between rip channel cross-sectional area and mean velocity, though velocity variability was not explored in detail.

Given the limited research into bathymetric controls on surfzone current variability, there are multiple hypotheses and relationships that require further investigation, notably, (i) the observations of Castelle et al. (2010) on the continuum in flow behavior between high- and low-three-dimensionality rip channels were confined to a lab experiment and require field verification across multiple scenarios; (ii) no statistical relationships have been demonstrated between bathymetric three-dimensionality and measures of flow variability (e.g., eddy velocity and directional standard deviation); (iii) the relationship between bathymetric three-dimensionality and mean flow behavior has been tested on a subjective point, the rip neck or bar crest, but has not been tested as a generalized relationship across the surfzone; and (iv) other aspects of bathymetric geometry (e.g., channel angle) have not been investigated, for example, that as channel obliquity increases, vorticity becomes biased toward one direction. Testing these relationships constitutes the aim of this study.

2. Field Sites

Field data were collected at three embayed beaches in the region of Sydney, Australia, (Figure 1a) between July and November 2012. Embayed beaches are a suitable environment for testing bathymetric controls on surfzone flow due to alongshore changes in beach state (Short, 1999) and the occurrence of “mega-rip” or embayment-cellular beach states (Castelle, Scott, et al., 2016), where deep rip channels can occur immediately adjacent to alongshore uniform morphology (Loureiro et al., 2012). The observed beaches were Whale Beach (McCarroll et al., 2014), Bondi Beach (McCarroll et al., 2016), and North Cronulla Beach (Van Leeuwen et al., 2015). The Sydney offshore wave climate is high energy with modal significant wave height $H_s = 1.6$ m and peak wave period $T_p = 10$ s from the SSE (Short & Trenaman, 1992). Tides are microtidal with mean spring tidal range of 1.6 m. Bondi Beach (Figures 1b and 1c) is deeply embayed, with medium-fine sand, 850-m long, facing SSE, fully exposed at the southwest end becoming protected at the northeast corner. During observations (McCarroll et al., 2016), a complex multibar system developed at the south end, grading to a low-tide-terrace at the northern end. Whale Beach (Figure 1d) is 600-m long, with medium-coarse sand, facing east with a protected southern corner. During field observations (McCarroll et al., 2014), the beach was configured with one large rip channel near the middle of the beach, small channels at either headland and importantly, a 300-m long alongshore uniform region at the midnorth of the beach. North Cronulla Beach (Figure 1e) is at the southern end of 10-km long Bate Bay, facing SE at the location of field observations, grading to greater wave exposure to the NE, with medium-fine sand. At the time of field observations (Van Leeuwen et al., 2015), the surfzone bathymetry was configured in a combination of transverse and rhythmic bars.

3. Methods

3.1. Field Observations

Observations at the three beaches include 2 days of Lagrangian drifter observations at Bondi (Figures 1b and 1c) and 1 day each at Whale (Figure 1d) and Cronulla (Figure 1e). Across the four days of field observations, seven zones were selected (Figures 1b–1e, black rectangles) with a three character code indicating the beach, deployment, and location along the beach (S-south; M-middle; and N-north), for example, B1S is Bondi-Deployment 1-South. Six zones were selected to encompass a rip channel and surrounding

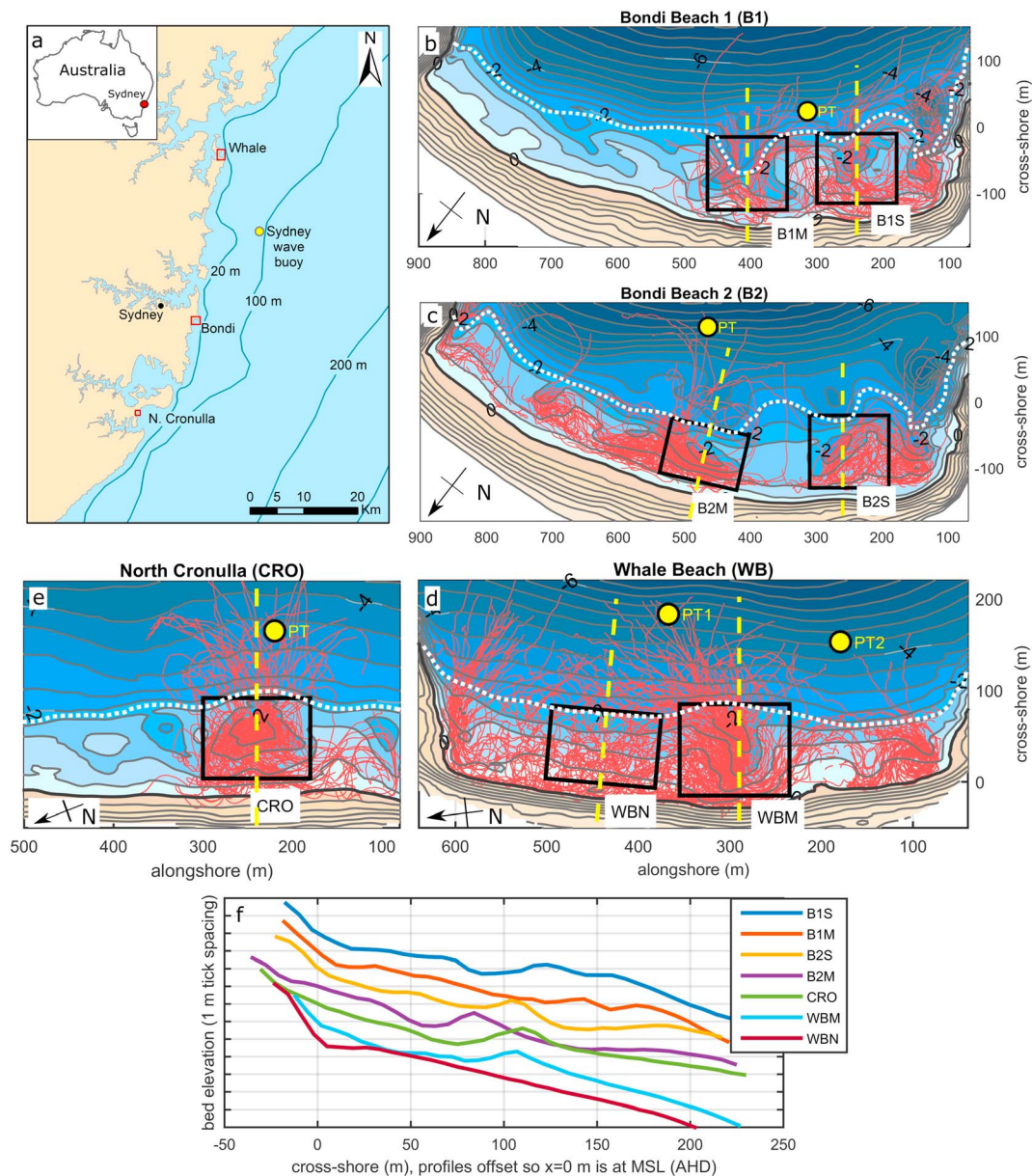


Figure 1. (a) Field sites, (b) Bondi Beach, deployment 1 (B1), (c) Bondi Beach, deployment 2 (B2), (d) Whale Beach, and (e) North Cronulla Beach. Pink tracks indicate drifter trajectories; black rectangles indicate seven flow regimes selected for analysis (B1M, B1S, B2M, B2S, WBM, WBN, and CRO). Drifter tracks outside these zones are not used in the analysis. For (b)–(e) the mean shoreline is bold ($z = 0$ m, MSL AHD71) and the approximate breakpoint line is white dotted. (f) Cross sections for each zone indicated by yellow dashed lines in (b)–(e).

bars within the surfzone. The remaining zone (WBN) is a relatively alongshore uniform region. These zones were selected to represent a variety of flow regimes, from deep rip channels to alongshore uniform morphology, with a range of rip channel obliquity. The alongshore extent of all flow regime zones was set to 120 m, sufficient to capture the morphological expression of a rip channel and adjacent bars. The cross-shore extent of flow regime zones is based on surfzone extent, varying from 80 to 110 m (mean 97 m), extending from the inner region of drifter coverage, excluding the swash zone, to the approximate edge of the surfzone. Further details on zone boundaries as they relate to statistical analysis, including sensitivity testing, are provided in section 3.5.

During drifter deployments, observations of wave height and period were derived from 1 or 2 pressure transducers (PTs) positioned on the bed, beyond the breakpoint in 3- to 6-m depth. Directional

Table 1
Field Experiment Deployment Information

Deployment	Waves (offshore)				Drifters			Flow regime zones			
	Date (2012)	Beach orientation	H_s (m)	T_p (s)	Dir. (deg.)	Duration (H:MM)	Drifter releases	Drifter hours	Tide (Range, AHD71)	ID	H_b (m)
Bondi (1)	26/07	SSE	1.3	10.7	110	2:42	119	26	Rising, over midtide (-0.2 m to 0.5 m)	B1S B1M	1.0 1.0
Bondi (2)	03/08	SSE	1.6	10.9	148	2:41	132	44	Falling, mid to low (0 to -0.6 m)	B2S B2M	1.5 1.4
Whale	04/10	E	1.1	12.7	160	4:47	293	107	Falling, high to mid-low (0.6 to -0.3 m)	WBM WBN	0.9 0.9
Cronulla	14/11	SE	1.4	10.2	150	3:15	109	41	Falling, over midtide (0.3 to -0.8 m)	CRO	0.8

spreading statistics were not collected. Lagrangian drifters were built to the specifications of MacMahan et al. (2009), with minor alterations as described in McCarroll et al. (2014). Nondifferential GPS units were used (McCarroll et al., 2014) logging at 1 Hz. Maximum position error was found to be <5 m, with a low-passed velocity root-mean-square error of O(0.01 m/s) when tested against a real-time-kinematic (RTK) survey grade Global Positioning System (GPS). Details for each deployment, including wave, tide, and drifter deployment information, are provided in Table 1. Wave height and peak period were derived from pressure data. Comparison of the PT locations (Figure 1) and previously described wave transformation models for Whale Beach (McCarroll et al., 2014) and Bondi Beach (McCarroll et al., 2016) indicated that the PT observations were at approximately the point of maximum wave shoaling prior to breaking; therefore, the PT-derived wave heights were used directly as breaking wave heights, without transformation. For Bondi 2 (Figure 1c), no PT was located offshore of zone B2S. However, a previously described wave transformation model (McCarroll et al., 2016) indicated an increase in wave height from B2M to B2S of 0.1 m; therefore, this higher breaking wave height value was used for B2S. Wave direction was not measured at the break point; however, all three beaches are equilibrium embayments where waves refract to nearshore normal at breaking, even for large offshore wave angles. This was previously demonstrated through MIKE21 wave models of Whale Beach (McCarroll et al., 2014) and for Bondi Beach (McCarroll et al., 2016). No numerical wave model exists for Cronulla, which is analogous to southern Monterey Bay, California, where breaking wave angle is persistently nearshore normal (MacMahan, Brown, et al., 2010). Observation durations varied in length, though all deployments covered a midtide period.

A maximum of 34 drifters were used during field observations, deployed primarily by field assistants near the shore or less frequently by personal water craft at the offshore surfzone limit. Drifters were deployed individually, rather than as groups, with an aim to maximize coverage across the domain. An effort was made to uniformly sample alongshore within a zone and to randomize deployment positions. At Bondi and Whale Beach the domain was the full extent of the embayment (Figures 1b–1d) and across a single rip cell at Cronulla (Figure 1e). Average deployment time across all sites for an individual drifter was 19 min.

Topo-bathymetric surveys were obtained using a personal watercraft (PWC) with mounted echo sounder and RTK-GPS for the sub- to lower intertidal, a backpack mounted RTK-GPS for the subaerial beach to upper intertidal, and a laser total station for the intertidal. The area of interest for drifter coverage was covered primarily by PWC survey. Mean repetitive differences for the PWC survey method are O(0.1 m) (MacMahan, 2001), while uncertainty values for the laser total station are less than 0.1 m. The backpack surveying method has greater uncertainty (O[0.2–0.3 m]) but only covered areas outside the zone of statistical analysis of bathymetric three-dimensionality. A maximum average alongshore spacing of 20 m was employed across all survey zones used in the analysis. Surveys were cleaned for outliers, merged, and linearly interpolated to a 5 m × 5 m grid. In order to remove noise at length scales less than the bathymetric features of interest (e.g., bars and rip channels), a weighted (1-cos²) smoothing function was applied to all bathymetric data sets across a five-point cross- and alongshore span.

3.2. Bathymetric Three-Dimensionality

Bathymetric three-dimensionality has previously been calculated as alongshore depth standard deviation (σ_d) (Feddersen & Guza, 2003). This approach is modified to a local bathymetric nonuniformity parameter (ϕ), which quantifies the alongshore bathymetric variability at any given location of the domain, rather than an alongshore mean. Additionally, the depth difference is taken from the depth value of the central point ($d[x_0, y_0]$) in the alongshore span being calculated (Δy), as opposed to an alongshore averaged value (Figure 2).

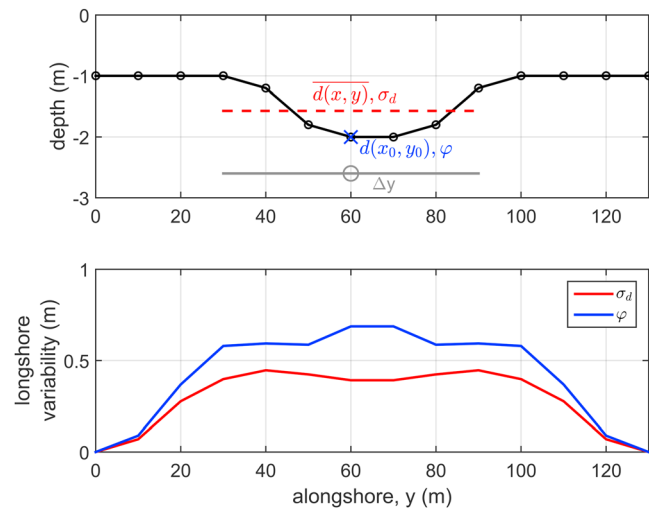


Figure 2. (top panel) alongshore profile of a rip channel, (bottom panel) alongshore variability evaluated at a moving alongshore position, using two methods. The σ_d method takes depth difference from an alongshore average ($\overline{d(x,y)}$), while the φ method takes the difference from the depth of the point being evaluated ($d(x_0, y_0)$).

$$\varphi(x, y) = \sqrt{\frac{1}{\Delta y} \int_{y-\Delta y/2}^{y+\Delta y/2} (d[x_0, y] - d[x_0, y_0])^2 dy} \quad (1)$$

This approach (φ) emphasizes extreme values, in particular the center of a rip channel, whereas the depth standard deviation (σ_h) can produce the highest values over transitions from bar to channel (Figure 2), depending on the alongshore scale Δy . This choice is motivated by the expectation that the channel midline will be a minima for dissipation and setup in the alongshore and by numerous observations showing that flow velocities have maximum values near the midline of the rip channel (e.g., Austin et al., 2010; MacMahan, Brown, et al., 2010). McCarroll et al. (2014) previously demonstrated using a similar technique that local variations in bathymetric variability, at alongshore scales <100 m, are important in forcing localized variations in mean velocity. For this study, an alongshore scale of 80 m was found to capture the scale of bars and channels of the observed sites. For replication purposes, this is approximately 80% of the average cross-shore extent of flow regime zones (Figure 1). As an additional verification of alongshore length scale selection, a sensitivity test was conducted across a range of Δy values (details in section 3.5). Bathymetric grids of 5 m were used across all field sites,

later interpolated to the 15 m grid used for flow variables (section 3.4) for statistical analysis. For clarity, the terms *bathymetric alongshore nonuniformity* and *three-dimensionality* are used interchangeably throughout the text.

3.3. Channel Angle

An objective, algorithmic method for determining channel angle was developed and applied across zones with rip channels (Figure 1, all zones excluding WBN). An example of this method applied to zone WBM is displayed in Figure 3, the channel angle is derived through the following steps: (i) calculating channel width, (ii) finding the channel midpoint, and (iii) calculating channel angle at multiple locations along the channel midline.

The width of the channel is defined here as the alongshore separation of a given *channel bounding contour* (c_{ch}), noting that this width varies based on the contour selected (Figure 3—red lines). There is no obvious single choice of contour to calculate width, so the method is repeated across three contours and later averaged. A base channel bounding contour is selected by examining all flow regime zones (Figure 1) and identifying the deepest common contour, at 0.2-m intervals, across all rip channels ($c_{ch} = -2.0$ m in this instance). This depth will be a function of wave and tide surfzone processes and will vary in other environments. The next two higher contours, at 0.2-m intervals, are also selected as channel bounding contours. In this case,

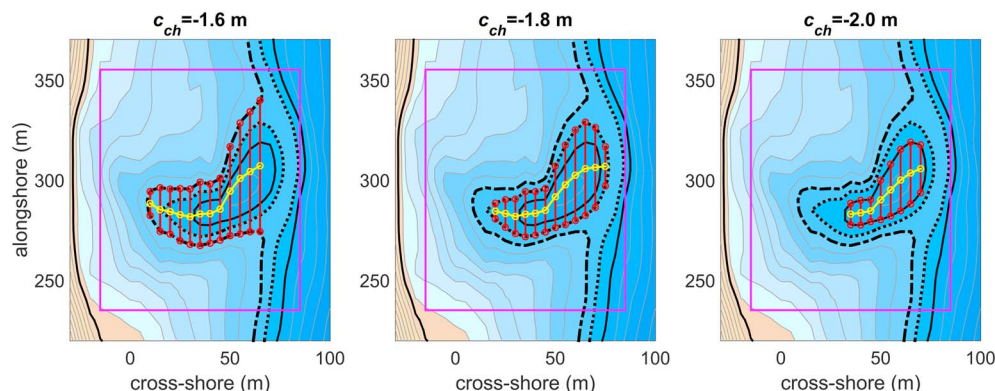


Figure 3. Channel angle algorithm applied to Whale Beach Mid zone (pink box), contours are at 0.2-m spacing with channel bounding contours highlighted ($c_{ch} = -1.6$ m, dash-dot; -1.8 m, dotted; -2.0 m, solid). Channel width intersection points and lines are red, with channel midline points and line in yellow.

the channel contours were $c_{ch} = -1.6, -1.8, \text{ and } -2.0$ m (Figure 3). This method of selecting multiple c_{ch} aims to reduce uncertainty by increasing the number of samples. The intuitive method of taking maximum depth at each cross-shore point was tested but produced poor results for high-angle channels. For B1M and CRO that have two distinct feeder channels (Figures 1b and 1e), the algorithm was run offshore of the point where the feeders merge into one rip neck. Once the channel bounding contours (c_{ch}) are identified, channel width can readily be calculated, and a simple three-point difference method is used to calculate channel angle at each position along the channel midline (Figure 3—yellow lines).

The method for determining mean channel angle is constructed around the hypothesis that channel angle will influence direction of eddy rotation. Channel alignment is 0° offshore, positive counterclockwise. The mean absolute channel angle (α) for a zone (e.g., WBM, Figure 3) was computed by averaging the absolute channel angle along the extent of the channel midlines of the three defined channel bounding contours:

$$\alpha = \frac{1}{n_\alpha} \sum_{k=1}^{n_\alpha} \alpha_{ch}(k) \quad (2)$$

where n_α is the number of channel angles for a given rip channel across all channel bounding contours. A measure of variability in channel obliquity is then taken as the standard deviation of channel angles:

$$\delta_\alpha = \sqrt{\frac{1}{n_\alpha - 1} \sum_{k=1}^{n_\alpha} (\alpha_{ch}(k) - \alpha)^2} \quad (3)$$

3.4. Lagrangian Drifter Analysis

Drifter data were preprocessed by filling data gaps, with a spline interpolation for gaps < 10 s and linearly for > 10 s. Gaps > 25 s were exceedingly rare (approximately one instance per 4 hr of drifter time). A 0.01-Hz low-pass third degree Butterworth filter was applied to all drifter data to exclude incident wave oscillations and the majority of infragravity bound and leaky waves, while retaining motions related to wave-forced transient surfzone eddies (Feddersen, 2014). Initial testing with a cutoff of 0.0067 Hz produced similar results, suggesting a degree of flexibility in filter cutoff selection. Data for each zone were rotated such that alongshore was parallel to the y axis when averaged over the zone (B2N and WBN were rotated from the orientation shown in Figure 1).

Instantaneous low-frequency drifter velocities were obtained through point-to-point difference in the cross shore ($u(x_{ij}, t)$) and alongshore ($v(x_{ij}, t)$), where x_{ij} is continuous position, and X_{ij} is a discrete bin location, the Cartesian axes (i, j) are subsequently omitted. Low-frequency mean velocity ($\bar{u}(X), \bar{v}(X)$) was calculated for $15 \text{ m} \times 15 \text{ m}$ bins across all field sites, with mean velocity magnitude ($U(X) = \sqrt{\bar{u}^2 + \bar{v}^2}$).

Low-frequency velocity variability was calculated similarly to Spydell et al. (2014), described as the transient eddy velocity. Anomalous low-passed velocities (u', v') at 1-Hz sampling intervals (t) are taken as the difference from the mean within each bin. For the cross-shore case:

$$u'(t|X) = u(t|X) - \bar{u}(X) \quad (4)$$

Low-frequency velocity standard deviation (σ_u) in the cross shore is then

$$\sigma_u(X) = \sqrt{\frac{1}{n-1} \sum (u')^2} \quad (5)$$

where n is the total number of all drifter observations within (X), with v' and σ_v obtained similarly. The eddy velocity magnitude is then ($\sigma_u(X) = \sqrt{\sigma_u^2 + \sigma_v^2}$). Instantaneous low-frequency drifter direction is the four-quadrant angle ($\theta = \tan^{-1}(v(t)/u(t))$). We opt to take an average of instantaneous directions, to avoid bias to high-velocity values dominating the calculation of mean direction. The first moment of a circular distribution (Berens, 2009) for each bin is

$$m_{1,\theta}(X) = \frac{1}{n} \sum \exp(i\theta(t|X)) \quad (6)$$

where $i = \sqrt{-1}$. Mean drifter trajectory in each bin is the angle:

Table 2
Number of Drifter Observations

Zone	Tracks	Total (n, 1 Hz)	Mean (n / grid cell)
B1S	51	12,273	435
B1M	49	17,092	281
B2S	32	18,525	403
B2M	47	41,182	1,085
CRO	82	69,013	1,526
WBM	131	57,857	1,345
WBN	68	58,804	1,363

$$\bar{\theta}(X) = \text{Arg}(m_{1,\theta}(X)) \quad (7)$$

A measure of the angular variability is the angular deviation, where vertical bars indicate absolute value:

$$\sigma_{\theta}(X) = \sqrt{2(1 - |m_{1,\theta}(X)|)} \quad (8)$$

The angular deviation has a maximum value of $\sqrt{2}$ radians for diametrically opposed directions and is equal to zero for unidirectional flow. Traditionally, instantaneous vertical vorticity is the curl of velocity:

$$\zeta = \nabla \times U = \frac{dv}{dx} - \frac{du}{dy} \quad (9)$$

A measure of instantaneous vorticity is required in order to address the relationship between channel angle and vorticity bias toward a preferred direction of rotation. When applying the traditional approach (9) to point-to-point drifter data, differential displacement and velocity values approach zero at times when a drifter is moving slowly, making the velocity curl approach unsuitable. As an alternative, a *rotation rate* (ζ), equivalent to vorticity for solid body rotation, is calculated as twice the low-frequency angular velocity ($\omega(x, t)$). This is taken as the differential change in angle, using point-to-point difference.

$$\zeta(t) = 2\omega(x, t) = 2 \frac{d\theta(x, t)}{dt} \quad (10)$$

For a given bin (X), the rotation bias ζ_{bias} is introduced as the ratio of drifter observations with positive (counterclockwise) rotation, scaled from $[-1$ to $+1]$. Thus, a value $\zeta_{\text{bias}} = -1$ indicates that all drifter observations have negative rotation, while $\zeta_{\text{bias}} = 1$ indicates 100% positive rotation.

$$\zeta_{\text{bias}}(X) = \frac{1}{n} \sum \text{sign}(\zeta_i(t|X)) \quad (11)$$

For all flow statistics, a minimum of 100 observations at 1 Hz were required per bin, to provide a sufficient distribution of velocities for statistical analysis. The number of drifter observations for each zone are given in Table 2, these are consistent with or exceed the sampling requirements outlined in previous studies (Spydell et al., 2007; MacMahan, Brown, et al., 2010).

3.5. Correlation Analyses

Statistical relationships were determined using two linear regression tests and a sensitivity analysis.

3.5.1. Correlation Test 1: Bathymetric Three-Dimensionality and Flow Behavior

Dependencies between flow variables were tested first ($U, \sigma_U, \sigma_{\theta}$). Next, we tested for correlations between bathymetric alongshore nonuniformity (φ) and the three flow variables. Both the “flow-flow” and “bathymetry-flow” tests were conducted using two complimentary methods: (i) discretized alongshore values, averaged in the cross shore; and (ii) mean values averaged across the flow regime zones (Figures 1b–1e, black rectangles).

Zone averages for each variable ($U, \sigma_U, \sigma_{\theta}, \varphi$) were determined by taking a mean of the bin-averaged values for a given variable, across each flow regime zone. For the discretized alongshore values, a cross-shore average of the binned values was taken at each alongshore position, at intervals of 15 m (the flow grid size). Taking cross-shore averaged values allows for comparison of different points along a given beach (cf. McCarroll et al., 2014). For example, $U_y(y)$ is the cross-shore averaged value for velocity magnitude, at each alongshore position. Variability across a zone is taken as the standard deviation of the averages at each cross-shore position (e.g., the standard deviation of U_y). Bathymetric nonuniformity (φ) is at higher resolution (5 m \times 5 m) and was linearly interpolated to the locations of the flow grid.

Mean and variable flow velocity is known to be positively correlated with wave forcing (e.g., MacMahan et al., 2006, 2004b); therefore, a method of scaling velocity by wave forcing is required to isolate the influence of bathymetry across multiple flow regimes. Rip current velocities (U_{rip}) have been shown (Bellotti, 2004) to scale with alongshore setup gradient ($U_{\text{rip}} \propto \sqrt{2g\Delta\eta_y}$) where g is gravity and $\Delta\eta_y$ is the alongshore water level gradient. Moulton et al. (2017) demonstrated that for moderate waves (“bar-break” conditions, applicable to

the observations in this study) that $\Delta\eta_y$ scales with breaking wave height (H_b). The relationship between transient eddy velocity and wave height is less evident, though recent work (Suanda & Feddersen, 2015) suggests that eddy velocity scales with $(\sqrt{gh_b})$, where h_b is breaking depth and directional spread. Breaking depth is proportional to breaking wave height through the break point parameter ($\gamma = H_b/h_b$), and directional spread was not measured in this study; therefore, it cannot be included in a normalization. Based on the above dynamic arguments, we opt to normalize velocities by $(\sqrt{gH_b})$, with the goal of removing the forcing control of waves on flow speeds. Nondimensional mean velocity is then $(\hat{U} = U/\sqrt{gH_b})$, and nondimensional velocity standard deviation is $(\hat{\sigma}_U = \sigma_U/\sqrt{gH_b})$.

The statistical methods introduced here must be robust and replicable, in particular where subjectivity is involved, for example, in zone selection. Accordingly, the following sensitivity tests were performed and are reported on briefly: (i) flow regime zone size for Correlation Test 1 was analyzed over a range of alongshore zone extents (70 to 160 m at 10-m intervals); (ii) alongshore span (Δy) for calculating bathymetric nonuniformity (φ , Correlation Test 1) was tested for three extents (60, 80, and 100 m); (iii) an alternative nondimensionalization to obtain \hat{U} and $\hat{\sigma}_U$ was performed, normalizing velocity and velocity standard deviation by (H_b/T_p) , similar to Brander (1999); and (iv) a nonuniform zone extent based on visual identification of "natural" morphological and hydrodynamic boundaries of the rip cell was tested.

3.5.2. Correlation Test 2: Channel Angle and Rotation Bias

This test is designed to detect a correlation between channel angle (α) and bias in direction of flow rotation (ζ_{bias}). Zone-averaged and cross-shore averaged values for ζ_{bias} were calculated as per the methods described above for other flow variables. Channel zone extent for Correlation Test 2 was tested for an initial value (same flow regime zone as Correlation Test 1) and then was sensitivity tested for a range of alongshore zone extents (70 to 160 m) to determine at what distances from the rip channel midline the relationship strengthens or attenuates.

4. Results

4.1. Bathymetric Observations

Three of the seven zones were selected as being exemplars of varying degrees of alongshore bathymetric variability and channel angle (Figure 4; WBN, B2M, and WBM). The exemplars represent the following: (i) an alongshore uniform beach (WBN) with minimal alongshore variability; (ii) a highly oblique, low three-dimensionality channel (B2M); and (iii) a deep, nearshore-normal channel (WBM). The three zones are used to provide spatial plots of the bathymetric and flow variables (sections 4.1 and 4.2), with summary statistics presented in tabular form for all sites. The remaining zones (B1S, B1M, B2S, and CRO) are required to provide statistical power in the correlation analysis (section 4.3) but are not examined in detail. Summary bathymetric statistics for all zones are given in Table 3.

4.2. Lagrangian Flow Observations

Combined drifter tracks, over the full deployment, with velocity and rotation rate (a proxy for vorticity) indicated are provided in Figure 5. Positive rotation rate indicates counterclockwise rotation. Three 10- to 20-min snapshots (Figure 6) of drifter activity give a qualitative indication of spatial flow variability over time, over the representative bathymetries. For the snapshots of WBM and B2M (Figure 6) drifters are only plotted if they are located in the rip neck at the start of the time block. Note that wave heights were greater at Bondi (B2M), than at Whale (WBM and WBN), which will be later accounted for by normalizing the velocity to account for the dependence of velocity on wave height (section 4.4).

Flow trajectories over the alongshore uniform zone (WBN, Figures 5a and 5d and 6a–6c) are characterized by seemingly random trajectories and vorticity, with occasional coherent surfzone eddies (e.g., Figure 6a, negative eddy at $y = 500$ m). Instantaneous velocities are generally low but are higher (up to 0.5 m/s) in the inner surfzone (Figure 5a).

The subtle, strongly oblique (i.e., high angle relative to shore normal) channel of B2M (Figures 5b and 5e and 6d–6f), appears to impose a substantial control on flow behavior, with positive vorticity eddies (matching the channel angle) oscillating along the inner channel margin (Figures 6d and 6e), at times exiting the surfzone (Figure 6f). Higher velocity, low vorticity trajectories are apparent near the center of the B2M channel

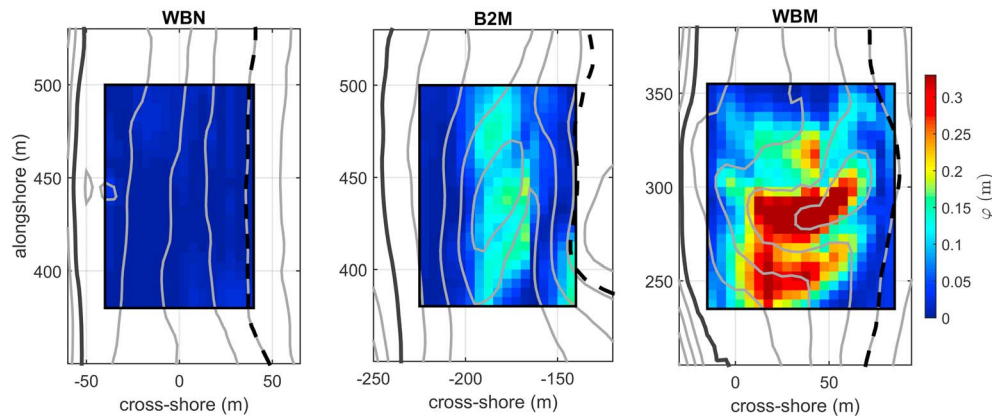


Figure 4. Alongshore bathymetric three-dimensionality ($\phi(m)$) for the exemplar zones (black boxes): Whale Beach-North (WBN), Bondi 2-Mid (B2M), and Whale Beach-Mid (WBM). Contours at 0.5-m spacing, $z = 0$ m is bold, black dashed line is approximate offshore limit of surfzone.

(Figure 5b), with the rotation rate tracks indicating a strong dominance of positive rotation along the extent of the channel (Figure 5e).

Flows through the deep, nearly shore normal WBM channel (Figures 5c and 5f and 6g–6i), exhibit high mean values (Figure 5c) with periodic changes in direction of rotation, appearing as an unstable jet exiting the surfzone (Figures 6g and 6h), before switching to high-vorticity rotation (Figure 6i). Examination of drifter animations (not shown) indicate that the flow does not simultaneously rotate in both directions but changes direction of rotation on the order of minutes.

4.3. Time-Averaged Synoptic Drifter Observations

The previous section presented instantaneous flow variables for qualitative assessment of bathymetric controls on flow behavior. This section provides binned values to examine time-averaged behavior. Mean velocity (U) and rotation direction bias (ζ_{bias}) are presented in Figure 7. For the alongshore uniform zone (WBN), mean U is uniformly low (Figure 7a) and ζ_{bias} is minimal (Figure 7d). The high-angle, low-relief channel (B2M) is characterized by moderate mean velocities, with a small area of high velocities at the center of the channel (Figure 7b). For the deep, near-normal channel (WBM, Figure 7c), a coherent path of high velocities extends from the southern feeder, through the channel to the offshore extent of the surfzone. The areas of high velocities for WBM are qualitatively correlated with local zones of high bathymetric three-dimensionality (Figure 4—right), suggesting localized velocity response to bathymetry (~50-m scale in the alongshore).

Flows in the B2M channel center and inner margin are strongly directionally biased (Figure 7e); however, the bottom-right corner is poorly sampled. In contrast, the center of the WBM channel shows low rotation bias (Figure 7f), with areas of high bias of opposing direction to either side of the channel. The B2M observations are consistent with positive eddies advecting/oscillating along the channel margin, while the WBM observations indicate an unstable rip neck flow that oscillates between positive rotation over the north bar and negative rotation over the south bar.

These observations inspire the hypothesis to test for a correlation between channel angle and vorticity bias in the immediate vicinity of rip channels.

Variability in flow velocity and direction is now examined (Figure 8). A clear spatial relationship is evident in velocity standard deviation (σ_U) over the alongshore uniform zone (Figure 8a), with values of 0.2 m/s in the inner surfzone decreasing to below 0.1 m/s at the outer surfzone and beyond. Furthermore, there appears to be a clear increase in σ_U at Whale Beach, transitioning from the alongshore uniform zone (WBN, Figure 8a) to the immediately adjacent rip channel (WBM, Figure 8c). This suggests a strong relationship between bathymetric nonuniformity and velocity variability; however, subsequent analysis will demonstrate that there is no linear correlation when multiple zones are examined (section 4.4).

Table 3
Zone Average of Bathymetric Variables

Zone	Bathy. 3D		Channel angle	
	ϕ (m)	δ_ϕ (m)	α (deg.)	δ_α (deg.)
B1S	0.14	± 0.03	-26	± 12
B1M	0.21	± 0.04	-12	± 29
B2S	0.09	± 0.02	-33	± 10
B2M	0.06	± 0.01	54	± 5.5
CRO	0.12	± 0.03	-2	± 29
WBM	0.13	± 0.06	21	± 15
WBN	0.01	± 0.00	—	—

Note. δ_{variable} is the standard deviation of cross-shore averaged values, for 15-m alongshore intervals across each flow regime zone.

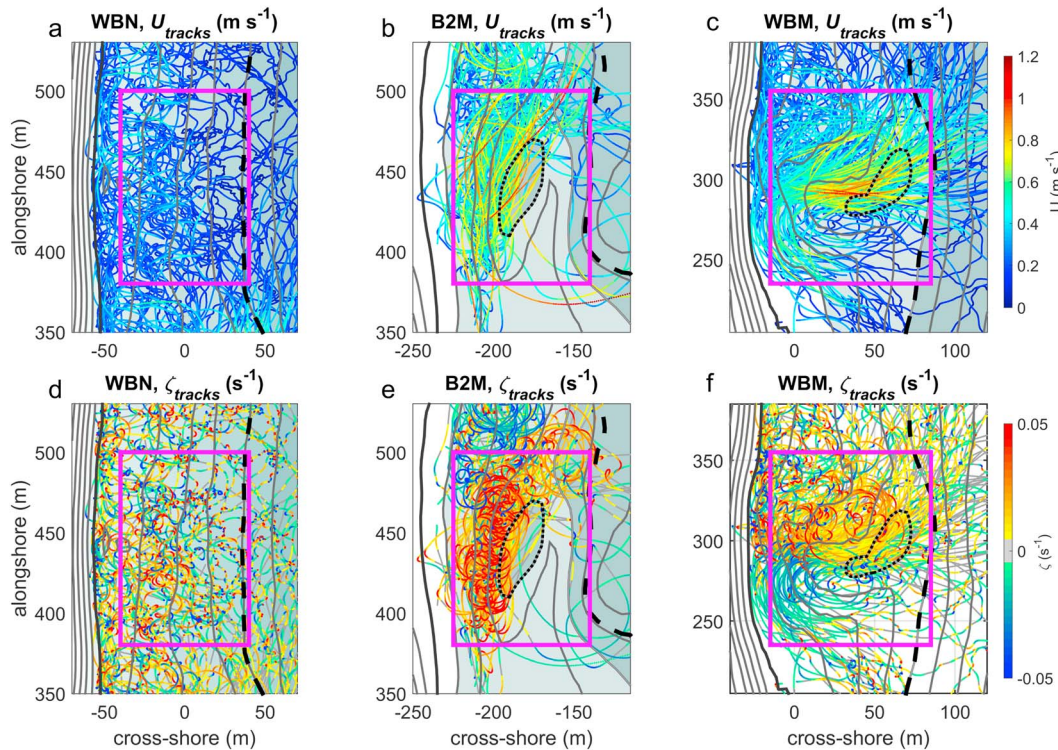


Figure 5. Instantaneous, low-frequency velocity tracks (top row) and rotation rate (bottom row), for the three representative zones (pink boxes; WBN, B2M, WBM). Contours at 0.5 m spacing, $z = 0$ m is bold, $z = -2$ -m rip channel contour is dotted, approximate limit of surfzone is dashed. WBN = Whale Beach-North; B2M = Bondi 2-Mid; WBM = Whale Beach-Mid.

Angular deviation (σ_θ) is uniformly high across the alongshore uniform zone (Figure 8d) and generally lowest in rip channels, in particular a small zone in the center of the B2M oblique channel (Figure 8e) and a large zone around the deep WBM channel and southern feeder (Figure 8f). Qualitatively, there appears to be a good inverse relationship between mean U (Figure 7—top row) and σ_θ (Figure 8—bottom row), with U generally higher over the deeper channel zone (WBM) and σ_θ higher over the alongshore uniform zone (WBN). Zone averaged values for U , ζ_{bias} , σ_U and σ_θ are given for all zones in Table 4.

4.4. Correlation Analysis

Correlation analyses are now undertaken to statistically verify the morphological and hydrodynamic relationships described in previous sections, with methods and rationale provided in section 3.5. As a preliminary task, the morphological relationship between bathymetric nonuniformity (φ) and channel angle (α) is examined (Figure 9). For the observed rip channels, bathymetric nonuniformity appears inversely correlated with absolute channel angle, peaking around shore normal (0°). This can be explained geometrically: as a channel becomes more oblique, it transitions into an alongshore feature with lower alongshore three-dimensionality, for example, an idealized longshore trough may be deep, but $\varphi = 0$. Therefore, there will be some natural limit on bathymetric three-dimensionality as channel angle increases, such that the top-right and top-left of Figure 9 will be unpopulated. However, a shallow shore-normal channel could occupy the lower-middle of the parameter space (Figure 9) but is not present in this data set (CRO is the closest to this morphology type).

4.4.1. Correlation Test 1: Flow and Bathymetric Three-Dimensionality

The first part of this test determines dependencies between the flow variables (Figure 10—left column). Flow velocity and velocity standard deviation (variable eddy velocity) are normalized to scale for wave forcing (e.g., $\hat{U} = U/\sqrt{gH_b}$). Linear correlations are tested for both the flow regime zone-averaged (120-m alongshore length) and cross-shore averaged values (15-m discretized alongshore spacing), with correlation results in Table 5. Error bars in Figure 10 indicate the standard deviation of the cross-shore averaged values.

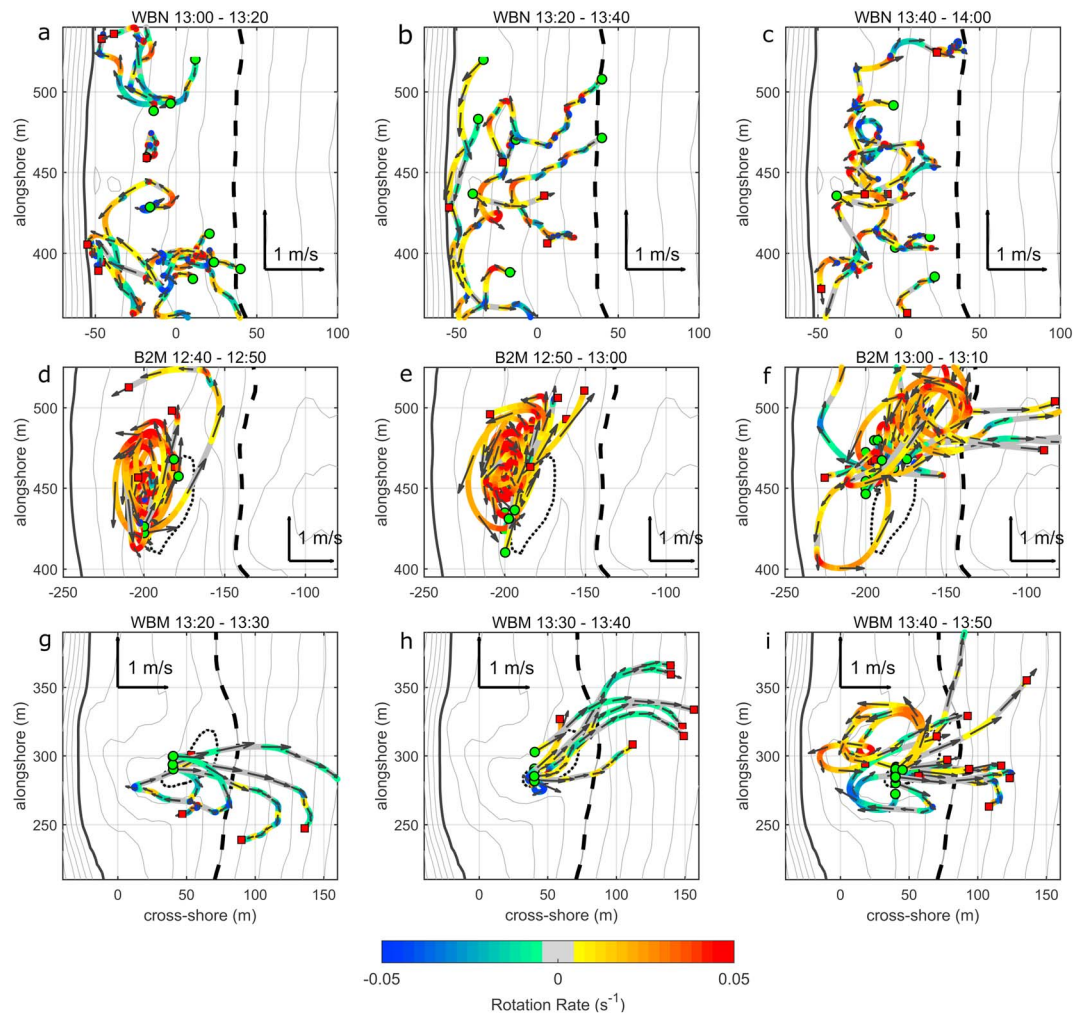


Figure 6. Ten to twenty minute time block snapshots for WBN (a–c), B2M (d–f), WBM (g–i). Drifter track color is rotation rate (ζ), with start point (green circle) and end point (red square) indicated. Vectors are drifter velocity, with scale indicated in each frame. Contours at 0.5-m spacing, $z = 0$ m is bold, $z = -2$ -m rip channel contour is dotted, approximate limit of surfzone is dashed. WBN = Whale Beach-North; B2M = Bondi 2-Mid; WBM = Whale Beach-Mid.

Initial testing for a linear correlation between normalized mean velocity (\hat{U}) and normalized velocity standard deviation ($\hat{\sigma}_U$) showed only a weak linear relationship (Figure 10a) that was not significant ($R^2 = 0.49$, $p = 0.08$) for zone-averaged values (large markers in Figure 10) and was weak but significant ($R^2 = 0.21$, $p < 0.001$) for the larger sample of cross-shore averaged values (small markers in Figure 10). However, a strong linear relationship ($R^2 = 0.95$) was found between \hat{U} and $(\hat{U}/\hat{\sigma}_U)$, such that $[\hat{\sigma}_U = \hat{U}/(0.115 + 10.7\hat{U})]$, shown as a red dotted line in Figure 10a. This implies that as mean velocity increases, velocity standard deviation initially increases at a faster rate than \hat{U} , but the rate of increase rapidly plateaus for $(\hat{U} > 0.03)$. Some caveats must be given regarding this approach: (i) $\hat{\sigma}_U$ can be nonzero when $\hat{U} = 0$, so the fit between these variables need not pass through the origin; (ii) if $\hat{\sigma}_U$ were constant, then Figure 10b is simply correlating \hat{U} with itself; and (iii) the logarithmic-type growth of $\hat{\sigma}_U$ (Figure 10a) depends heavily on a single point (WBN), while for all other zones ($\hat{\sigma}_U \approx 0.08$), therefore the conclusions that can be drawn as to precise scaling of $\hat{\sigma}_U$ are limited.

A strong linear correlation was also found between \hat{U} and angular deviation (σ_θ) (Figure 10c), with $[\sigma_\theta = 1.23 - 5.41\hat{U}]$ for the zone-averaged values. To further test the dependence between flow variables (\hat{U} , $\hat{\sigma}_U$, σ_θ), we generated a synthetic distribution of directional deviation ($\sigma_{\theta, syn}$), using equations (6) to (8), for values of \hat{U} between 0 and 0.15, with assumptions that (i) $\hat{\sigma}_U$ is dependent on \hat{U} (as per Figure 10b); and

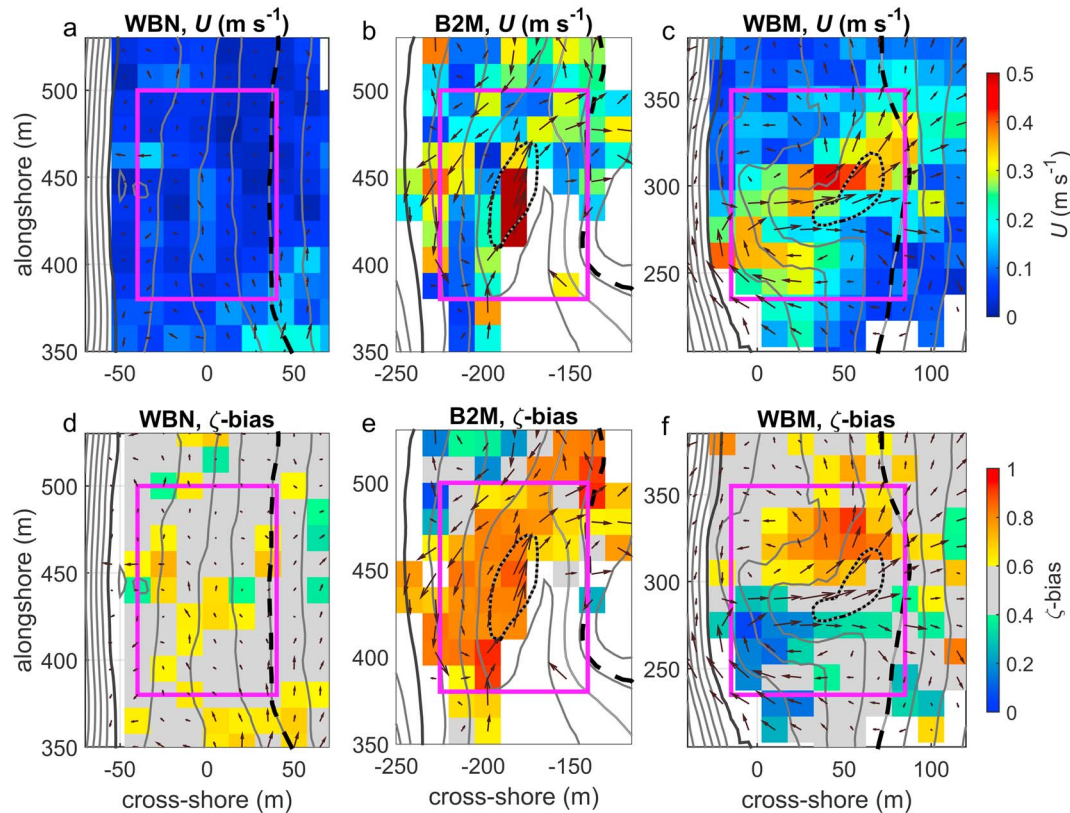


Figure 7. Mean velocity (U ; a–c) and rotation bias (ζ_{bias} ; d–f), for the three representative zones (pink boxes; WBN, B2M, and WBM). Vectors indicate mean velocity in all panels. WBN = Whale Beach-North; B2M = Bondi 2-Mid; WBM = Whale Beach-Mid.

(ii) cross- and alongshore velocities $[u, v]$ have Gaussian distribution with equal standard deviation $[\sigma_u = \sigma_v = \widehat{\sigma}_U/\sqrt{2}]$. A linear fit of $[\sigma_{\theta, \text{syn}} = 1.30 - 6.10\widehat{U}]$ was found to be suitable for small values of \widehat{U} , though we note that a nonlinear curve would be required for $(\widehat{U} > 0.2)$. The fit for $\sigma_{\theta, \text{syn}}$ (red dotted line, Figure 10c) is near identical to the fit for σ_{θ} (black dashed line, Figure 10c), suggesting all three flow variables are interdependent to some degree.

This second part of the test quantifies the influence of bathymetric nonuniformity (φ) on flow behavior (Figure 10—right column). Mean velocity (\widehat{U}) was significantly correlated with φ at the zone-averaged level (Figure 10d Table 5; $R^2 = 0.76$). For cross-shore averaged values (small markers in Figure 10) the trend is still strong, though with more scatter about the trend line for higher φ values (e.g., B1M).

Variable eddy velocity ($\widehat{\sigma}_U$) was found to have no significant linear correlation with φ in all tests (Figure 10e and Table 5), including all the sensitivity tests outlined below. However, a significant relationship was found between φ and $(\widehat{U}/\widehat{\sigma}_U)$ (Figure 10f), consistent with the relationship between \widehat{U} and $(\widehat{U}/\widehat{\sigma}_U)$ (Figure 10b). It is clear that the strength of this relationship is primarily based on the correlation between \widehat{U} and φ (cf. Figure 10d), so the relationship between $\widehat{\sigma}_U$ and φ is inconclusive. Bathymetric variability was strongly correlated with directional variability (Figure 10g), though now with an inverse correlation ($r = -0.90$), as expected given the relationship between \widehat{U} and σ_{θ} (Figure 10c).

It is notable that the bathymetry-flow tests (Figure 10—right column) are significant across the zone-average test as well as the discretized (15 m) cross-shore averaged segments, implying that these relationships are robust and persistent at varying spatial scales. The increase in scatter for higher φ values (Figure 10—right column) indicates that there is a lower correlation between bathymetry and flow response for highly 3-D systems at high spatial resolution but that when averaged out over a larger zone, the relationships are robust.

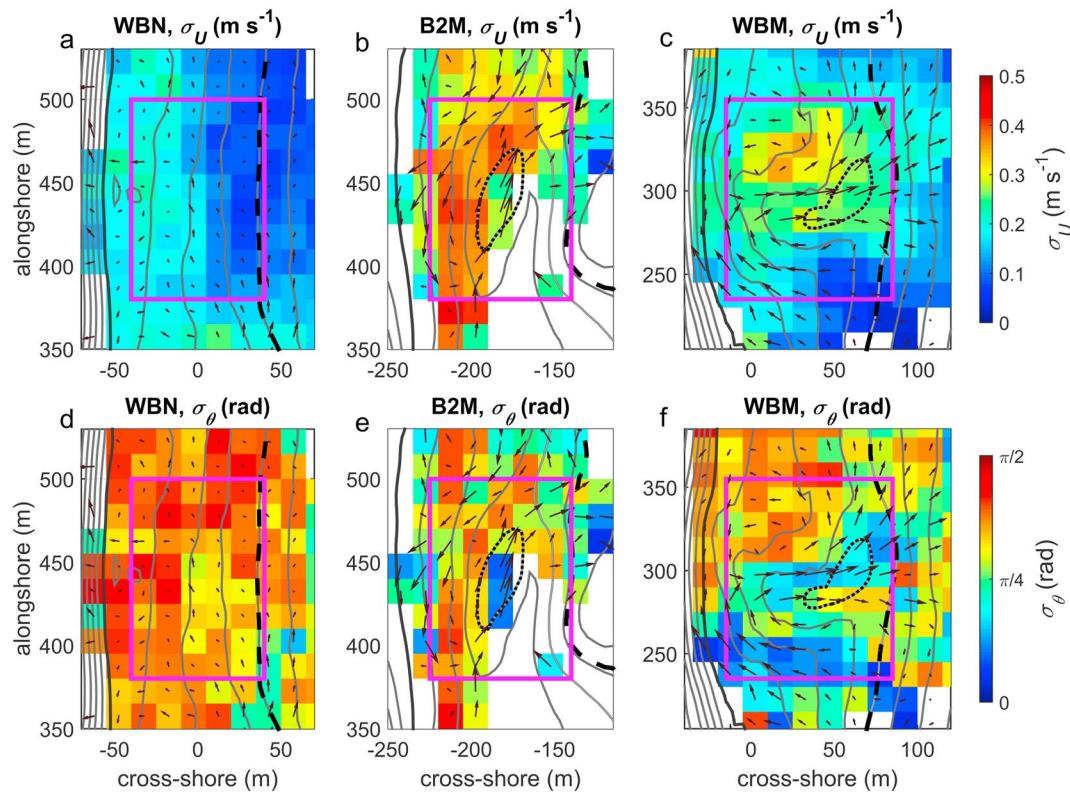


Figure 8. Velocity standard deviation (σ_U ; a–c) and angular deviation (σ_θ ; d–f), for the three representative zones (pink boxes; WBN, B2M, and WBM). Contours at 0.5-m spacing, $z = 0$ m is bold, $z = -2$ -m contour is dashed. Vectors indicate mean velocity. WBN = Whale Beach-North; B2M = Bondi 2-Mid; WBM = Whale Beach-Mid.

The novel methods presented in this study require a number of subjective decisions in regard to zone selection and alongshore length scales. In order to test the robustness of the statistical outcomes and to assist in replicability, a series of sensitivity tests were conducted. First, the alongshore extent of the “flow regime zone” was varied (from 70 to 160 m at 10-m intervals). Second, the alongshore span for calculating φ was varied (60, 80, and 100 m). Across both these tests, the bathymetry-flow correlations (Figure 10—right column) remained persistent ($0.68 < R^2 < 0.86$; for zone-averaged values). All relationships increased slightly in strength for greater zone width.

A third sensitivity test involved an alternative nondimensionalization to obtain \hat{U} , normalizing velocity and velocity standard deviation by (H_b/T_p) . In this instance the φ and \hat{U} relationship was very strong ($R^2 = 0.92$),

while the φ and \hat{U}/σ_U was unchanged ($R^2 = 0.8$). A fourth sensitivity test used nonuniform zone extent based on visual identification of “natural” morphological and hydrodynamic boundaries of the rip cell. For instance, the zone around B1M (Figure 1b) had greater alongshore extent due to the width of this rip channel. Again, the results were near identical to the initial test shown in Figures 10d–10f.

To summarize the flow and bathymetric three-dimensionality analyses, based on the spatially averaged values across the seven zones: (i) flow variables were found to be nonindependent, in particular $[\sigma_\theta^\alpha - \hat{U}]$; (ii) flow variables were correlated with bathymetric three-dimensionality, such that $[\hat{U}^\alpha \varphi]$ and $[\sigma_\theta^\alpha - \varphi]$; and (iii) $\hat{\sigma}_U$ was not linearly correlated with \hat{U} or φ , but nonlinear growth of $\hat{\sigma}_U$ is suggested with $[\hat{\sigma}_U \propto \hat{U} / (a + b\hat{U})]$, where a and b are positive constants.

Table 4
Zone Averaged Flow Variables

Zone	Mean velocity		Rotation bias		Velocity St. Dev.		Angular deviation	
	U	δU	ζ_{bias}	$\delta\zeta - \text{bias}$	σ_U	$\delta\sigma_U$	σ_θ	$\delta\sigma_\theta$
B1S	0.29	0.09	0.53	0.20	0.28	0.03	44	8.7
B1M	0.35	0.06	0.40	0.16	0.26	0.04	37	6.4
B2S	0.34	0.06	0.32	0.09	0.31	0.07	42	8.4
B2M	0.23	0.06	0.74	0.09	0.34	0.02	55	6.1
CRO	0.17	0.04	0.46	0.16	0.23	0.01	50	6.0
WBM	0.21	0.06	0.53	0.19	0.22	0.06	42	13
WBN	0.05	0.01	0.53	0.04	0.15	0.01	66	4.1

Note. δ_{variable} is the standard deviation of cross-shore averages for a given variable at 15-m alongshore intervals.

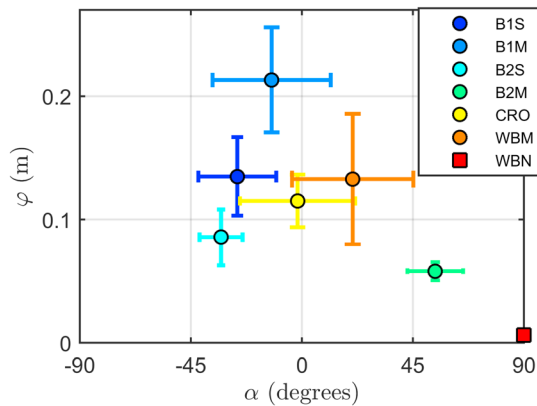


Figure 9. Channel angle and bathymetric nonuniformity. WBN (alongshore uniform) is given a theoretical angle of 90°. x -error bars for α are 1 standard deviation of the channel angles evaluated along the channel midline, y -error bars are the standard deviation of cross-shore averaged values for ϕ . WBN = Whale Beach-North; B2M = Bondi 2-Mid; WBM = Whale Beach-Mid.

4.4.2. Correlation Test 2: Channel Angle and Rotation Bias

Next, the influence of channel angle (α) on rotation bias (ζ_{bias}) is tested (Figure 11). Binned values (15 m \times 15 m) for ζ_{bias} are averaged over the flow regime zones (Figure 1). A sensitivity test on the α and ζ_{bias} relationship was conducted by varying the alongshore zone width from 70 to 160 m. The alongshore uniform region (WBN) is included for reference but is qualitatively uncorrelated with the rip channelled regions. A strong correlation ($R^2 = 0.93$) is observed between channel angle with rotation bias for zone width of 70 m (Figure 11a), with a near-linear increase in the coefficient of determination as the zone width is reduced (Figure 11b). For the 120-m zone width, that is, the zones used for the above “flow-bathymetry” correlations, the correlation is weaker but significant ($R^2 = 0.73$) and becomes nonsignificant for zone widths ≥ 140 m.

The higher angle channels (B2S and B2M) are correlated with greater rotation bias (Figure 11a), in the direction of channel angle. The channels that are closer to shore normal (B1S, B1M, WBM, and CRO) have minimal rotation bias (values close to 0) and greater variability (larger error bars). This strongly suggests that rip channels exert a significant control on flow rotation and that this control is strongest in the immediate vicinity of the channel. It must be noted that the two zones with higher channel angles have gaps in the sampling coverage (Figure 1c, SE corner of B2S, SW corner of B2M), where rotation could be expected to be occurring in the opposite direction, potentially reducing ζ_{bias} to values closer to 0. The unsampled areas account for <25% of the total area. However, at lower zone widths, the correlation is apparent even when B2S and B2M are excluded from the regression ($R^2 = 0.79$, $p = 0.1$, for zone width 70 m), providing additional support for the relationship.

It is evident that the channel angle and rotation bias relationship (Figures 11a and 11b) will only be linear over some limited range of increasing channel angle, as extreme oblique (high angle) channels eventually transition into alongshore troughs or alongshore uniform regions (e.g., WBN, in Figure 11a) that exert no control over direction of flow rotation. Therefore, we expect a two-phase relationship: first, as channel angle increases from shore normal, rotation bias increases, but for the end-member alongshore uniform zone (WBN), ζ_{bias} approaches zero. An attempt is made to linearize this two-phase relationship by taking the difference of the absolute value of the channel angle from 45°, described as “channel obliquity” ($||\alpha| - 45^\circ|$). The use of 45° is roughly inferred from Figure 11a as a first approximation. We then take an absolute form of rotation bias $|\zeta_{\text{bias}}|$, where 0 indicates random eddy direction and 1 indicates uniform direction of rotation. As for all variables in the correlation analyses, $|\zeta_{\text{bias}}|$ is calculated for individual grid cells and then averaged across the zone.

The linearized relationship (Figure 11c) is weaker than the signed version (Figures 11a and 11b), but importantly, it addresses the full spectrum of morphological scenarios. This implies that high oblique channel angle forces a preferred direction of eddy rotation (e.g., B2M), compared to both transverse channels (e.g., WBM) and alongshore uniform morphology (WBN). Large error bars and limited spread of the data (Figure 11) preclude definitive determination of the ideal angle that maximizes ζ_{bias} ; however, the general two-phase trend described above is well supported by a combination of spatial observations (sections 4.3 and 4.4) and correlation analysis. A sensitivity analysis on the $|\zeta_{\text{bias}}|$ and “channel obliquity” relationship (Figure 11d) broadly shows an increasing trend as zone width decreases, though with more noise than Figure 11b.

The linearized relationship (Figure 11c) is weaker than the signed version (Figures 11a and 11b), but importantly, it addresses the full spectrum of morphological scenarios. This implies that high oblique channel angle forces a preferred direction of eddy rotation (e.g., B2M), compared to both transverse channels (e.g., WBM) and alongshore uniform morphology (WBN). Large error bars and limited spread of the data (Figure 11) preclude definitive determination of the ideal angle that maximizes ζ_{bias} ; however, the general two-phase trend described above is well supported by a combination of spatial observations (sections 4.3 and 4.4) and correlation analysis. A sensitivity analysis on the $|\zeta_{\text{bias}}|$ and “channel obliquity” relationship (Figure 11d) broadly shows an increasing trend as zone width decreases, though with more noise than Figure 11b.

To summarize the relationships between channel angle and rotation bias, (i) the signed version of the relationship (Figures 11a and 11b) is statistically robust but fails to incorporate alongshore uniform regions, and (ii) the absolute version of the relationship, based on the difference in channel angle from 45° (Figures 11c and 11d), is less robust (weaker correlations and larger error bars) but crucially demonstrates the entire morphological sequence. Further, some areas of the high-angled channels (B2S and B2M) have incomplete sampling coverage. However, if all the analyses are taken together, including the synoptic observations (Figures 5–7) and both statistical tests (Figure 11), these support the hypothesis of a morphohydrodynamic spectrum from: (i) shore normal rip channels with low rotation bias within the channel; to (ii) high

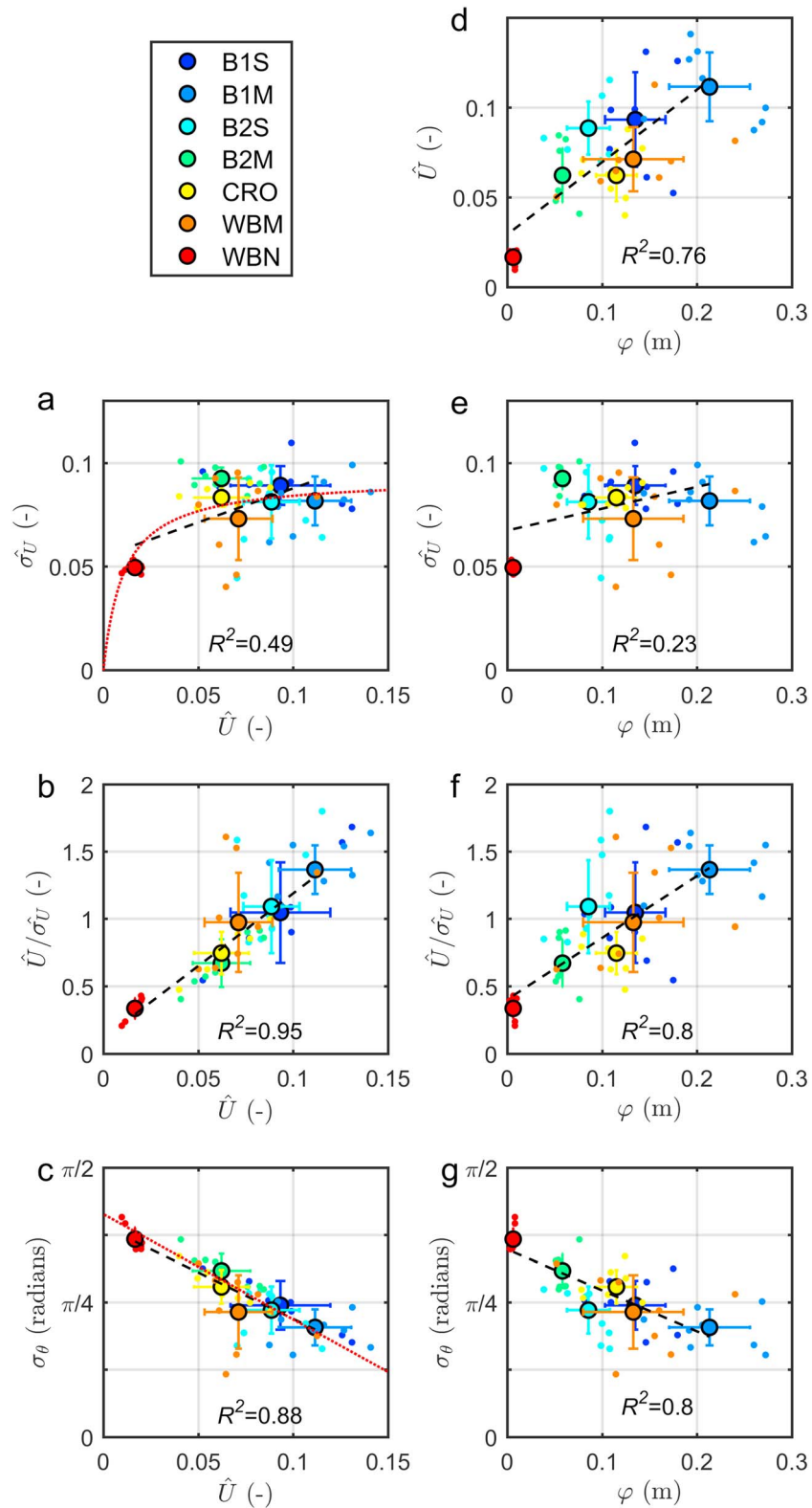


Figure 10. Correlation analysis for “flow-flow” relationships (a–c) and “flow-bathymetry” relationships (d–g). Large circles with black borders are flow-regime zone-averaged values of binned variables; small markers are cross-shore average values at 15-m spacing in the alongshore. Black dashed lines are linear trend lines for the zone-averaged values, with associated R^2 values given. Error bars are described in the text. Red dotted lines in (a) and (c) are derived from the linear correlation in (b).

Table 5
Flow and Bathymetric Three-Dimensionality Correlations

Figure 10	Var. 1	Var. 2	Zone-averaged values				Cross-shore averaged, 15-m intervals	
			p value	R^2	Equation		p value	R^2
					Intercept	Gradient		
a	\hat{U}	$\hat{\sigma}_U$	0.079	0.49	0.05	0.33	<0.001	0.21
b	\hat{U}	$\hat{U}/\hat{\sigma}_U$	<0.001	0.95	0.11	10.73	<0.001	0.74
c	\hat{U}	σ_θ	0.002	0.88	1.23	-5.41	<0.001	0.64
d	φ	\hat{U}	0.011	0.76	0.03	0.40	<0.001	0.46
e	φ	$\hat{\sigma}_U$	0.271	0.23	0.07	0.11	0.079	0.06
f	φ	$\hat{U}/\hat{\sigma}_U$	0.006	0.80	0.40	4.57	<0.001	0.45
g	φ	σ_θ	0.006	0.80	1.09	-2.39	<0.001	0.47

oblique channels with high rotation bias within the channel; and to (iii) alongshore uniform regions with near-zero rotation bias.

5. Discussion

It has been demonstrated that bathymetry exerts multiple controls on surfzone rotational currents, including (i) strong control over mean velocity and directional variability and (ii) control over bias in direction of flow rotation, through variations in channel angle. The findings are now contextualized against other research and are summarized in a conceptual model (Figure 12) illustrating how rotational currents within the

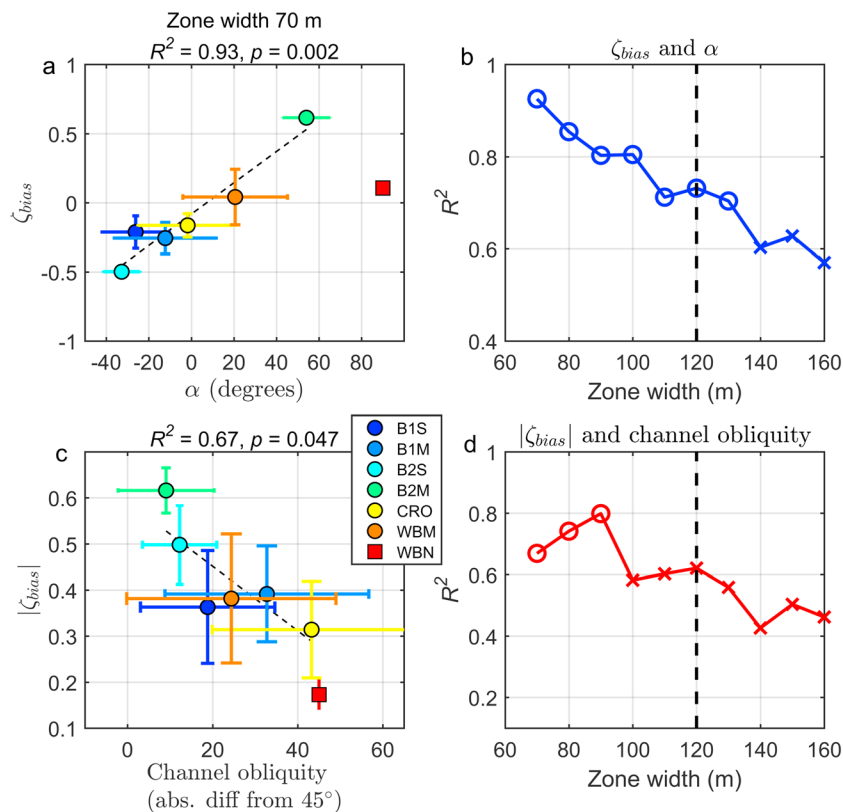


Figure 11. Channel angle correlation analysis, (a) channel angle and zone-averaged rotation bias (b) sensitivity test for relationship in (a) at a range of zone widths, (c) absolute value formulation of channel angle (channel obliquity) and rotation bias, (d) sensitivity test for panel (c). For (a) and (b), WBN (alongshore uniform zone) is included in the plot for reference with $\alpha = 90^\circ$ but is excluded from the correlation analysis; black dashed lines are linear trend lines, x-error bars are 1 standard deviation of the channel angles evaluated along the channel midline (absolute angles used for [c]), y-error bars are the standard deviation of cross shore averaged values of rotation bias at 15-m alongshore intervals. For (b) and (d) open circles indicate $p \leq 0.05$, crosses indicate $p > 0.05$, vertical dashed line at 120 m indicates the zone width used in section 4.4.1.

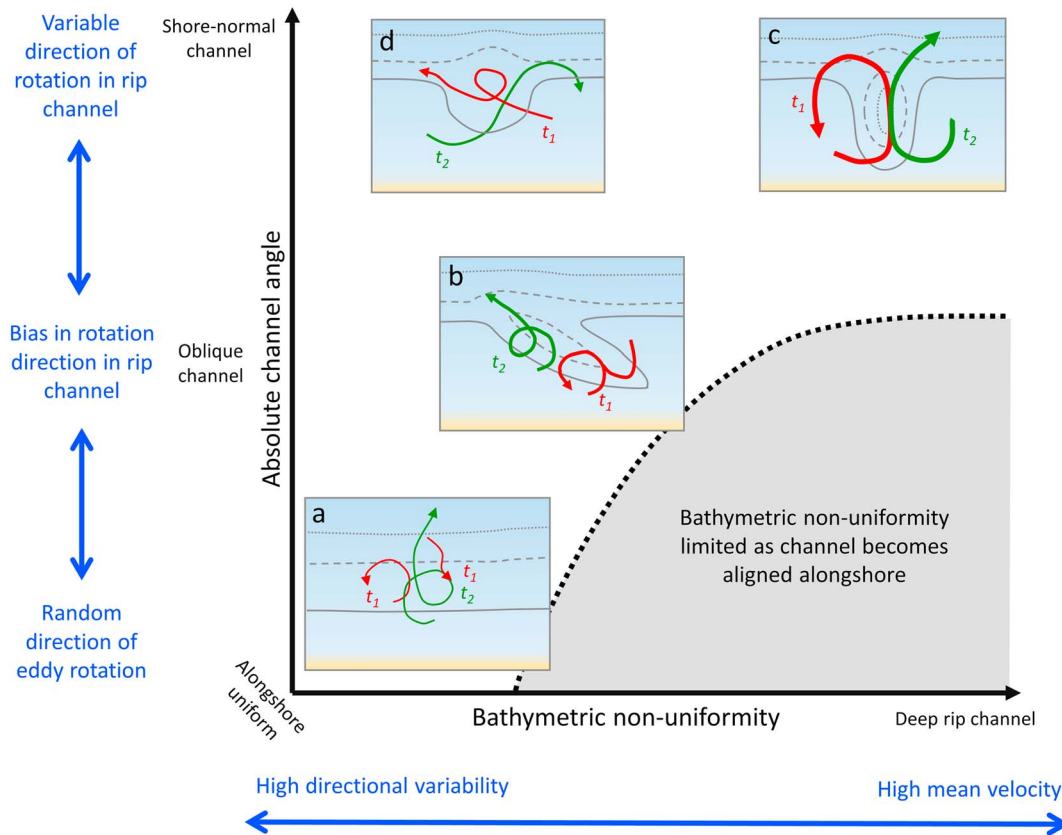


Figure 12. Conceptual model of bathymetric controls on flow within the surfzone, flow arrow (red and green) widths indicate relative current velocity, t_1 and t_2 indicate subsequent time periods, minutes apart. (a)–(c) are similar to flow regimes observed in this study; (d) is a predicted flow regime, not directly observed in this study but most similar to CRO.

surfzone vary with changes in bathymetry. This model is intended for use in making broad assumptions about the type of flow that will occur over a given bathymetry, potentially with only visual observations. It is anticipated that a simplified version of this model may be of use to beach safety practitioners who deal with surfzone currents as a bathing hazard (e.g., Castelle, McCarroll, et al., 2016; McCarroll et al., 2015). Bathymetric controls are presented on two axes, bathymetric nonuniformity (horizontal) and channel angle (vertical), with idealized bathymetries illustrating typical flow behavior. Three of the flow regimes are similar to the exemplar zones in this study (Figures 12a–12c), and the final flow regime predicts flow behavior in a shallow, shore-normal channel (Figure 12d), not observed in this study.

The strongest relationship is that as bathymetric nonuniformity (φ) increases (Figures 12a to 12c), flow behavior shifts from high directional variability ($\hat{\sigma}_\theta$) to high mean velocity (\hat{U}). This is consistent with previous efforts that have observed the relationship between channel depth and flow velocity (Austin et al., 2010; Brander & Short, 2001; Castelle et al., 2010; MacMahan et al., 2006). Earlier efforts to establish a relationship between bathymetric variability and flow velocity tended toward using single point measurements for velocity in the channel (e.g., Castelle et al., 2010). These approaches are analogous to the “cross-shore averaged” values we use in the bathymetry three-dimensionality and flow analysis (Figure 10, small symbols). McCarroll et al. (2014) initially established the relationship between bathymetric variability and flow velocity along the extent of a single beach (Whale Beach), the present effort generalizes this relationship across multiple beaches with varying bathymetries and wave conditions.

We argue that our approach of taking “zone averages” is a more robust, universal approach to determine flow velocity on any given bathymetry. Similarly, the demonstrated relationship between φ and flow directional variability is consistent with Castelle et al. (2010). In particular, we note that the correlation ($\hat{U} \propto \varphi$) and conversely ($\sigma_\theta \propto -\varphi$) are impressively persistent across a range of spatial scales ($R^2 > 0.7$ for zone width 80 to 160 m), with marginally stronger relationships at greater zone width. A primary contribution of this effort

is to link mean velocity with directional variability and to demonstrate the spectrum of behavior from along-shore uniform morphology to deep rip channels, using field observations across multiple sites.

Less clear was the response of velocity variability ($\hat{\sigma}_U$), which was greater over the rip-channeled zones than the alongshore uniform zone, but no linear relationship was found between bathymetric nonuniformity and $\hat{\sigma}_U$ (Figure 10b and Table 5). A nonlinear relationship was suggested with $[\hat{\sigma}_U \propto \hat{U} / (a + b\hat{U})]$ but if this relationship is to be verified, more observations of low three-dimensionality beaches are required, or alternatively a phase-resolving model (e.g., Feddersen, 2014) could be used to test the scaling of $\hat{\sigma}_U$. Our results are therefore only partially consistent with the numerical modeling results of Reniers et al. (2007), which indicated that velocity variability increased with bathymetric variability, and similarly with Castelle et al. (2010), who observed in a laboratory model that rips “pulse” more with higher bathymetric variability.

The precise relationship between bathymetric variability and flow velocity variability appears to be nonlinear, and the mechanisms for the interaction are yet to be clearly explained. Wave directional spreading was not measured and therefore could not be accounted for in the correlation analysis. Directional spreading is necessary for generating transient surf zone eddies (Peregrine, 1998) and is positively correlated with low-frequency velocity standard deviation (MacMahan, Reniers, et al., 2010) and vorticity variability (Spydell & Feddersen, 2009). To further elucidate the relationship between bathymetric variability, directional spreading and eddy velocity (i.e., σ_U), future observations must account for all of these components.

Next, we examine the vertical axis of the conceptual model (Figure 12), with channel angle relative to shore normal. Our initial hypothesis was that bathymetric nonuniformity would only partly explain variability of rotational currents within the surfzone and that other aspects of bathymetric geometry would also influence flow behavior. Previous efforts have incorporated rip channel cross-sectional area (Austin et al., 2010; Brander, 1999), slope (Suanda & Feddersen, 2015), rip spacing (Kennedy et al., 2006; MacMahan et al., 2006), and the presence of rip head bars (Castelle et al., 2014) but have done little to examine channel angle. The findings of this study suggest a nonlinear relationship between channel angle and preferred direction of current rotation in the rip channel (ζ_{bias}). Over an alongshore uniform zone, there is no preferred direction of rotation (Figure 13a), with randomly directed transient eddies forced purely by hydrodynamics (e.g., Clark et al., 2012). A novel finding of the present effort is that moderate- to high-oblique channel angle appears to force a strongly preferred direction of flow rotation in the rip neck. This was supported by analysis of flow behavior (Figures 5–7) and a correlation test (Figure 11), though some data gaps (e.g., Figure 7e, B2M) limit the conclusiveness of the statistical result.

The control on eddy direction of the center of the channel is likely due to waves driving flow over the onshore bar. As channel angle becomes shore normal (Figure 12c), there is no bathymetric control on flow direction in the rip neck and small changes in wave direction will force the flow to change direction of rotation, consistent with the lab observations of Kennedy and Thomas (2004). Similarly, if a slight alongshore current is present, eddy direction may be biased (Wilson et al., 2013) and intermittent breaking will introduce sufficient vorticity for a current to switch between alongshore meandering and rip cell rotation (Houser et al., 2013). Other factors that may affect eddy bias not addressed here include asymmetric bar height on each side of the channel and alongshore pressure gradients. More field observations are required to confirm the hypothesized relationship from shore normal rip channels (low rotation bias), to high oblique-channels (high rotation bias), and to alongshore uniform regions (near-zero rotation bias).

An absent rip type in the observations of this study was a shallow, shore-normal channel (e.g., Castelle et al., 2010; MacMahan et al., 2008), with CRO being the closest observed channel to these criteria (Figure 9). An idealized channel of this type is included in the conceptual model (Figure 13d), where it is predicted that flows will be highly directionally variable, with low (though nonzero) mean velocities and no preferred direction of rotation in the rip neck.

The methods described here are applicable to beaches with shore normal wave exposure, typical for equilibrium bays, but would require modification for surfzones with mean alongshore currents (e.g., Feddersen, 2014; Houser et al., 2013; Moulton et al., 2017; Winter et al., 2014), as no attempt is made to differentiate forcing from localized alongshore breaking wave height gradients and that of a mean oblique wave direction. This was the case for an additional zone that was briefly examined but was subsequently excluded from the analysis (Figure 1c, $y = 720$ m in the alongshore), as it was found to have anomalously high

alongshore currents (McCarroll et al., 2017) up to 0.5 m/s, potentially due to a strong offshore (beyond the surfzone) wave height gradient in that region. Wilson et al. (2013) identified that at the length scales of rip cells (hundreds of meters) advection from alongshore currents can act to dampen offshore-directed rip velocities. It is possible that even slight alongshore currents (e.g., Whale Beach, McCarroll et al., 2014) may have marginally impacted on rip flows, accounting for a component of variability not covered by our approach.

Water level variations are not accounted for in this study, despite tidal levels exerting substantial changes in flow patterns (Austin et al., 2010; Scott et al., 2014). The beaches examined here are all from the same microtidal coast, and drifter observations were all made at similar tidal levels. However, even small changes in water level can account for variations in flow patterns and intensity (e.g., McCarroll et al., 2014), such that a component of the flow variability not accounted for by bathymetry (Figure 10—right column) is likely the result of water level impacts. If the methods presented here were applied to beaches with substantially different tidal levels or at one mesotidal-macrotidal location at different tidal levels, then water level would need to be incorporated into the various correlation analyses and parameterizations.

6. Conclusions

The aim of this study was to identify bathymetric controls on surfzone flow behavior. Using a multibeach data set, seven “flow regimes” across three beaches were examined using fleets of Lagrangian drifters. Six of these zones contained rip channels of varying morphologies; the seventh zone was alongshore uniform. Bathymetry was characterized by a measure of alongshore nonuniformity and by channel angle relative to shore normal. Flow dynamics were analyzed by mean velocity, low-frequency velocity standard deviation, and low-frequency directional variability (angular deviation) as well as by preferred direction of low-frequency eddy rotation (rotation bias). Flow velocity and standard deviation were nondimensionalized by $(\sqrt{gH_b})$ to scale for the influence of wave forcing.

While several efforts have examined variability at the seaward extent of rip channels in the form of retention rates, few studies have explored flow variability over 3-D bathymetry *within* the surfzone. Now, two broad areas of research into rotational currents within the surfzone have been synthesized: (i) investigations into rip currents on 3-D bathymetry and (ii) examinations of transient surfzone eddies on alongshore uniform bathymetry.

The key findings of this study are the following:

1. A robust relationship exists between bathymetric variability, nondimensionalized mean flow velocity and directional variability. As surfzone bathymetry becomes more alongshore variable, mean flow increases and flow directional variability decreases. This appears to be a linear relationship extending from alongshore uniform morphology to deeply incised channels.
2. No significant linear relationship was found between bathymetric variability and flow velocity variability. However, the alongshore uniform zone did have lower velocity variability than the rip-channeled zones, implying nonlinear growth of velocity variability with bathymetric variability. The prior hypothesis of deeply channelized rips “pulsing” more than shallow rips was not clearly supported. A clearer elucidation of the mechanisms involved and further field observations are required.
3. Channel angle was found to be correlated with rotation bias within the rip channel. For alongshore uniform regions, eddy rotation direction is random, forced purely by hydrodynamic controls. Rotation bias was strongest within rip channels at a high oblique angle to the shoreline. For shore-normal channels, rotation is directionally biased over the bars and feeder channels adjacent to the rip, but flow frequently changes direction of rotation in the rip neck.

Finally, we introduced a conceptual model to synthesize the major findings such that they can be broadly applied to predict flow regimes on similar beaches. This study demonstrates that transient eddies and mean flow in channelized rip currents should not be treated as separate entities. The forcing mechanisms of both rely on alongshore differences in wave dissipation and are differentiated by the persistence of each mechanism over time. When examined jointly, over a range of bathymetries, we see a continuum of behavior from random eddies over alongshore uniform morphology to strong mean flows in deep channels, with aspects of flow mediated by the geometry of the channel.

Acknowledgments

This project was funded by the Australian Research Council (ARC) Linkage Project LP110200134, Surf Life Saving Australia and by Agence National de la Recherche (ANR), grant ANR-17-CE01-0014. Many thanks those who helped with the fieldwork, including Ian Turner, Ben Van Leeuwen, Hannah Power, Melissa Bracs, Kristen Splinter, Josh Scott, Len Martin, Mark Davidson, Murray Copas, the student volunteers of UNSW, the Waverley, Pittwater and Sutherland Shire Council lifeguards and the Australian Lifeguard Service. Sydney and Port Kembla wave buoy and Sydney tidal gauge data were provided by Manly Hydraulics Lab on behalf of the NSW Office of Environment and Heritage. Topobathymetry and drifter data analyzed in this manuscript are available as supporting information linked to the online version of this article. We warmly thank the reviewers for their substantial contributions to the improvement of this manuscript.

References

- Austin, M., Scott, T., Brown, J., Brown, J., MacMahan, J., Masselink, G., & Russell, P. (2010). Temporal observations of rip current circulation on a macro-tidal beach. *Continental Shelf Research*, *30*(9), 1149–1165.
- Bellotti, G. (2004). A simplified model of rip currents systems around discontinuous submerged barriers. *Coastal Engineering*, *51*(4), 323–335. <https://doi.org/10.1016/j.coastaleng.2004.04.001>
- Berens, P. (2009). CircStat: A MATLAB toolbox for circular statistics. *Journal of Statistical Software*, *31*(10), 1–21.
- Bonneton, P., Bruneau, N., Castelle, B., & Marche, F. (2010). Large-scale vorticity generation due to dissipating waves in the surf zone. *Discrete and Continuous Dynamical Systems, Series B*, *13*(4), 729–738. <https://doi.org/10.3934/dcdsb.2010.13.729>
- Bowen, A. J. (1969). Rip currents: 1. Theoretical investigations. *Journal of Geophysical Research*, *74*, 5467–5478. <https://doi.org/10.1029/JC074i023p05467>
- Brander, R. W. (1999). Field observations on the morphodynamic evolution of a low-energy rip current system. *Marine Geology*, *157*(3–4), 199–217. [https://doi.org/10.1016/S0025-3227\(98\)00152-2](https://doi.org/10.1016/S0025-3227(98)00152-2)
- Brander, R. W., & Short, A. D. (2000). Morphodynamics of a large-scale rip current system at Muriwai Beach, New Zealand. *Marine Geology*, *165*(1–4), 27–39.
- Brander, R. W., & Short, A. D. (2001). Flow kinematics of low-energy rip current systems. *Journal of Coastal Research*, *17*(2), 468–481.
- Bruneau, N., Bonneton, P., Castelle, B., & Pedreros, R. (2011). Modeling rip current circulations and vorticity in a high-energy mesotidal-macrotidal environment. *Journal of Geophysical Research*, *116*, C07026. <https://doi.org/10.1029/2010JC006693>
- Bruneau, N., Castelle, B., Bonneton, P., Pedreros, R., Almar, R., Bonneton, N., et al. (2009). Field observations of an evolving rip current on a meso-macrotidal well-developed inner bar and rip morphology. *Continental Shelf Research*, *29*, 1650–1662.
- Castelle, B., McCarroll, R., Brander, R., Scott, T., & Dubarbier, B. (2016). Modelling the alongshore variability of optimum rip current escape strategies on a multiple rip-channelled beach. *Natural Hazards*, *81*, 664–686.
- Castelle, B., Michallet, H., Marieu, V., Leckler, F., Dubardier, B., Lambert, A., et al. (2010). Laboratory experiment on rip current circulations over a moveable bed: Drifter measurements. *Journal of Geophysical Research*, *115*, C12008. <https://doi.org/10.1029/2010JC006343>
- Castelle, B., Reniers, A., & MacMahan, J. (2014). Bathymetric control of surf zone retention on a rip-channelled beach. *Ocean Dynamics*, *64*(8), 1221–1231. <https://doi.org/10.1007/s10236-014-0747-0>
- Castelle, B., Scott, T., Brander, R., & McCarroll, R. (2016). Rip current types, circulation and hazard. *Earth-Science Reviews*, *163*, 1–21. <https://doi.org/10.1016/j.earscirev.2016.09.008>
- Clark, D. B., Elgar, S., & Raubenheimer, B. (2012). Vorticity generation by short-crested wave breaking. *Geophysical Research Letters*, *39*, L24604. <https://doi.org/10.1029/2012GL054034>
- Dalrymple, R. A., MacMahan, J. H., Reniers, A. J. H. M., & Nelko, V. (2011). Rip currents. *Annual Review of Fluid Mechanics*, *43*, 551–581.
- Feddersen, F. (2014). The generation of surfzone eddies in a strong alongshore current. *Journal of Physical Oceanography*, *44*(2), 600–617. <https://doi.org/10.1175/JPO-D-13-051.1>
- Feddersen, F., & Guza, R. (2003). Observations of nearshore circulation: Alongshore uniformity. *Journal of Geophysical Research*, *108*(C1), 3006. <https://doi.org/10.1029/2001JC001293>
- Hally-Rosendahl, K., Feddersen, F., Clark, D. B., & Guza, R. (2015). Surfzone to inner-shelf exchange estimated from dye tracer balances. *Journal of Geophysical Research: Oceans*, *120*, 6289–6308. <https://doi.org/10.1002/2015JC010844>
- Houser, C., Arnott, R., Ulzhöfer, S., & Barrett, G. (2013). Nearshore circulation over transverse bar and rip morphology with oblique wave forcing. *Earth Surface Processes and Landforms*, *38*(11), 1269–1279. <https://doi.org/10.1002/esp.3413>
- Johnson, D., & Pattiaratchi, C. (2004). Transient rip currents and nearshore circulation on a swell-dominated beach. *Journal of Geophysical Research*, *109*, C02026. <https://doi.org/10.1029/2003JC001798>
- Johnson, D., & Pattiaratchi, C. (2006). Boussinesq modelling of transient rip currents. *Coastal Engineering*, *53*(5–6), 419–439. <https://doi.org/10.1016/j.coastaleng.2005.11.005>
- Kennedy, A., Brocchini, M., Soldini, L., & Gutierrez, E. (2006). Topographically controlled, breaking-wave-induced macrovortices. Part 2. Changing geometries. *Journal of Fluid Mechanics*, *559*, 57–80. <https://doi.org/10.1017/S0022112006009979>
- Kennedy, A. B., & Thomas, D. (2004). Drifter measurements in a laboratory rip current. *Journal of Geophysical Research*, *109*, C08005. <https://doi.org/10.1029/2003JC001927>
- Kumar, N., & Feddersen, F. (2017). The effect of Stokes drift and transient rip currents on the inner shelf. Part II: With stratification. *Journal of Physical Oceanography*, *47*(1), 243–260. <https://doi.org/10.1175/JPO-D-16-0077.1>
- Longuet-Higgins, M. S., & Stewart, R. W. (1964). Radiation stresses in water waves; a physical discussion, with applications. *Deep Sea Research and Oceanographic Abstracts*, *11*(4), 529–562. [https://doi.org/10.1016/0011-7471\(64\)90001-4](https://doi.org/10.1016/0011-7471(64)90001-4)
- Loureiro, C., Ferreira, Ó., & Cooper, J. A. G. (2012). Extreme erosion on high-energy embayed beaches: Influence of megarips and storm grouping. *Geomorphology*, *139–140*, 155–171. <https://doi.org/10.1016/j.geomorph.2011.10.013>
- MacMahan, J. (2001). Hydrographic surveying from personal watercraft. *Journal of Surveying Engineering*, *127*(1), 12–24. [https://doi.org/10.1061/\(ASCE\)0733-9453\(2001\)127:1\(12\)](https://doi.org/10.1061/(ASCE)0733-9453(2001)127:1(12))
- MacMahan, J., Brown, J., Brown, J., Thornton, E., Reniers, A., Stanton, T., et al. (2010). Mean Lagrangian flow behavior on an open coast rip-channelled beach: A new perspective. *Marine Geology*, *268*(1–4), 1–15. <https://doi.org/10.1016/j.margeo.2009.09.011>
- MacMahan, J., Brown, J., & Thornton, E. (2009). Low-cost handheld global positioning system for measuring surf-zone currents. *Journal of Coastal Research*, *25*(3), 744–754.
- MacMahan, J., Thornton, E., Stanton, T., & Reniers, A. (2005). RIFEX: Observations of a rip current system. *Marine Geology*, *218*(1–4), 113–134. <https://doi.org/10.1016/j.margeo.2005.03.019>
- MacMahan, J. H., Reniers, A. J., & Thornton, E. B. (2010). Vortical surf zone velocity fluctuations with 0 (10) min period. *Journal of Geophysical Research*, *115*, C06007. <https://doi.org/10.1029/2009JC005383>
- MacMahan, J. H., Reniers, A. J., Thornton, E. B., & Stanton, T. P. (2004a). Infragravity rip current pulsations. *Journal of Geophysical Research*, *109*(C1), C01033. <https://doi.org/10.1029/2003JC002068>
- MacMahan, J. H., Reniers, A. J., Thornton, E. B., & Stanton, T. P. (2004b). Surf zone eddies coupled with rip current morphology. *Journal of Geophysical Research*, *109*, C07004. <https://doi.org/10.1029/2003JC002083>
- MacMahan, J. H., Thornton, E. B., & Reniers, A. J. (2006). Rip current review. *Coastal Engineering*, *53*(2–3), 191–208. <https://doi.org/10.1016/j.coastaleng.2005.10.009>
- MacMahan, J. H., Thornton, E. B., Reniers, A. J., Stanton, T. P., & Symonds, G. (2008). Low-energy rip currents associated with small bathymetric variations. *Marine Geology*, *255*(3–4), 156–164. <https://doi.org/10.1016/j.margeo.2008.08.006>

- McCarroll, R. J., Brander, R., & Scott, T. (2017). Wave height and bathymetric controls on surfzone current velocity and dispersion across an embayed beach. *Coastal Dynamics 2017* (pp. 431–442). Helsingor, Denmark.
- McCarroll, R. J., Brander, R. W., Turner, I. L., Power, H. E., & Mortlock, T. R. (2014). Lagrangian observations of circulation on an embayed beach with headland rip currents. *Marine Geology*, *355*, 173–188. <https://doi.org/10.1016/j.margeo.2014.05.020>
- McCarroll, R. J., Brander, R. W., Turner, I. L., & Van Leeuwen, B. (2016). Shoreface storm morphodynamics and mega-rip evolution at an embayed beach: Bondi Beach, NSW, Australia. *Continental Shelf Research*, *116*, 74–88. <https://doi.org/10.1016/j.csr.2016.01.013>
- McCarroll, R. J., Castelle, B., Brander, R. W., & Scott, T. (2015). Modelling rip current flow and bather escape strategies across a transverse bar and rip channel morphology. *Geomorphology*, *246*, 502–518. <https://doi.org/10.1016/j.geomorph.2015.06.041>
- Moulton, M., Elgar, S., Raubenheimer, B., Warner, J. C., & Kumar, N. (2017). Rip currents and alongshore flows in single channels dredged in the surf zone. *Journal of Geophysical Research, Oceans*, *122*, 3799–3816. <https://doi.org/10.1002/2016JC012222>
- Peregrine, D. (1998). Surf zone currents. *Theoretical and Computational Fluid Dynamics*, *10*(1–4), 295–309. <https://doi.org/10.1007/s001620050065>
- Pitman, S., Gallop, S. L., Haigh, I. D., Masselink, G., & Ranasinghe, R. (2016). Wave breaking patterns control rip current flow regimes and surfzone retention. *Marine Geology*, *382*, 176–190. <https://doi.org/10.1016/j.margeo.2016.10.016>
- Reniers, A., MacMahan, J., Thornton, E., & Stanton, T. (2007). Modeling of very low frequency motions during RIXEX. *Journal of Geophysical Research*, *112*, C07013. <https://doi.org/10.1029/2005JC003122>
- Reniers, A. J., MacMahan, J., Thornton, E., Stanton, T., Henriquez, M., Brown, J., et al. (2009). Surf zone surface retention on a rip-channeled beach. *Journal of Geophysical Research*, *114*, C10010. <https://doi.org/10.1029/2008JC005153>
- Scott, T., Masselink, G., Austin, M. J., & Russell, P. (2014). Controls on macrotidal rip current circulation and hazard. *Geomorphology*, *214*, 198–215. <https://doi.org/10.1016/j.geomorph.2014.02.005>
- Short, A. D. (1999). *Handbook of beach and shoreface morphodynamics*. Great Britain: John Wiley.
- Short, A. D., & Trenaman, N. (1992). Wave climate of the Sydney region, an energetic and highly variable ocean wave regime. *Marine and Freshwater Research*, *43*(4), 765–791. <https://doi.org/10.1071/MF9920765>
- Sonu, C. J. (1972). Field observation of nearshore circulation and meandering currents. *Journal of Geophysical Research*, *77*, 3232–3247. <https://doi.org/10.1029/JC077i018p03232>
- Spydell, M., & Feddersen, F. (2009). Lagrangian drifter dispersion in the surf zone: Directionally spread, normally incident waves. *Journal of Physical Oceanography*, *39*(4), 809–830. <https://doi.org/10.1175/2008JPO3892.1>
- Spydell, M., Feddersen, F., Guza, R. T., & Schmidt, W. E. (2007). Observing surf-zone dispersion with drifters. *Journal of Physical Oceanography*, *37*(12), 2920–2939. <https://doi.org/10.1175/2007jpo3580.1>
- Spydell, M. S., Feddersen, F., Guza, R., & MacMahan, J. (2014). Relating Lagrangian and Eulerian horizontal eddy statistics in the surfzone. *Journal of Geophysical Research: Oceans*, *119*, 1022–1037. <https://doi.org/10.1002/2013JC009415>
- Suanda, S. H., & Feddersen, F. (2015). A self-similar scaling for cross-shelf exchange driven by transient rip currents. *Geophysical Research Letters*, *42*, 5427–5434. <https://doi.org/10.1002/2015GL063944>
- Van Leeuwen, B. R., McCarroll, R. J., Brander, R. W., Turner, I. L., Power, H. E., & Bradstreet, A. J. (2015). Examining rip current escape strategies in non-traditional beach morphologies. *Natural Hazards*, *81*, 145–165.
- Wilson, G. W., Özkan-Haller, H., & Holman, R. A. (2013). Quantifying the length-scale dependence of surf zone advection. *Journal of Geophysical Research: Oceans*, *118*, 2393–2407. <https://doi.org/10.1002/jgrc.20190>
- Winter, G., van Dongeren, A., de Schipper, M., & van Thiel de Vries, J. (2014). Rip currents under obliquely incident wind waves and tidal longshore currents. *Coastal Engineering*, *89*, 106–119. <https://doi.org/10.1016/j.coastaleng.2014.04.001>
- Yu, J., & Slinn, D. N. (2003). Effects of wave-current interaction on rip currents. *Journal of Geophysical Research*, *108*(C3), 3088. <https://doi.org/10.1029/2001JC001105>